International Journal of Climatology

International Journal of Climatology RMetS

RESEARCH ARTICLE

India's Drought Challenge: Insights From CMIP6 Models on Historical and Future Climate Scenarios

Rajeev Bhatla[1,2] | Aashna Verma[1] | Akash Vishwakarma[1] | R. K. Mall[2]

[1]Department of Geophysics, Institute of Science, Banaras Hindu University, Varanasi, India | [2]DST-Mahamana Centre of Excellence in Climate Change Research, Institute of Environment and Sustainable Development, Banaras Hindu University, Varanasi, India

Correspondence: Rajeev Bhatla (rbhatla@bhu.ac.in)

Received: 14 October 2024 | **Revised:** 30 April 2025 | **Accepted:** 23 July 2025

Keywords: climate scenarios | coupled model Intercomparison project phase 6 (CMIP6) | drought | standardised precipitation index (SPI)

ABSTRACT

Droughts, wielding devastating impacts on India, serve as the focal point of this research paper that explores key facets of India and its six distinct homogeneous regions' future climate by investigating the frequency, intensity, and underlying mechanisms of droughts. Utilising 10 General Circulation Models (GCMs) from the Coupled Model Intercomparison Project Phase 6 (CMIP6), spanning 1901 to 2014, our study employs a Multi-Model Ensemble (MME) approach under Shared Socioeconomic Pathways: SSP245 and SSP585 scenarios for the near (2031–2060) and far (2071–2100) future. Examining historical and projected scenarios, our findings reveal shifting patterns in drought frequency and intensity across regions, identifying North-west India (NWI) and North-central India (NCI) as potential hotspots. The study delves into atmospheric dynamics, revealing their role in drought vulnerabilities. Future trends under SSP245 and SSP585 trajectories underscore the impact of anthropogenic activities, with SSP585 projecting heightened drought risks, especially in NWI and NCI. The analysis of atmospheric physics uncovers the influence of moisture, convective processes, and regional climatic factors, attributing intensified drought risks to amplified atmospheric instability, particularly in NWI. Near-future precipitation patterns reflect regional nuances driven by atmospheric physics and climatic factors. Transitioning to the far future reveals persistent precipitation patterns, emphasising the role of emission trajectories in shaping drought conditions. Statistical analyses indicate an increase in drought intensity and duration, with NWI witnessing the maximum number of extreme droughts. Divergent regional patterns necessitate planned, adaptive policies to address evolving climate dynamics.

1 | Introduction

Droughts have emerged as one of the most challenging and impactful phenomena which pose a multifaceted challenge as a natural disaster, characterised by its complex nature that defies simple definition (Wilhite and Glantz 1985; Lloyd-Hughes 2014; Van Loon 2015). It encompasses various factors such as insufficient rainfall, depleted soil moisture, reduced streamflow, diminished vegetation vitality, and socioeconomic factors (Wilhite and Glantz 1985; Mishra and Singh 2010; Zargar et al. 2011). Defining droughts has long been a topic of serious debate; however, the Indian Meteorological Department (IMD) classifies India as drought-affected as a whole when the region receiving rainfall with a deficiency of 26% or more covers more than 20% of the total country area. Droughts exhibit remarkable variability in terms of their onset, duration, and spatial extent, driven by a complex influence of meteorological, hydrological, and environmental factors. Due to these factors, droughts are broadly classified into four types: meteorological, agricultural, hydrological, and socio-economic drought (Mishra and Singh 2010). This complexity poses challenges in characterising and predicting drought patterns. As per the studies concluded by Parthasarathy et al. (1994); Rajeevan et al. (2008) and Preethi

et al. (2019), India has witnessed a growing frequency of droughts. Approximately one-third of India's landmass consists of semi-arid and arid tropical regions, rendering the country highly susceptible to recurrent droughts and desertification (Nagarajan 2003).

The connection between water deficit and climate moisture deficits in various environments is complex and varied. So, it becomes quite challenging to accurately predict how droughts will spread in the future due to climate change (AghaKouchak et al. 2015). Furthermore, whilst there has been extensive research into drought trends over recent decades (Mishra and Liu 2014; Mallya et al. 2016; Bisht et al. 2019; Sharma and Goyal 2020; Verma et al. 2023), the exploration of future drought projections in India is still ongoing. Many studies have examined drought projections for India as a whole, yet there is a notable gap in accounting for the spatial variability and regional study of drought projections. In this study, therefore, the aim is to offer a thorough understanding of drought trends across India and its distinct homogeneous regions by the end of the 21st century by means of a drought indicator based on the result of a multi-model ensemble of 10 high-resolution climate projection models. The advancement of drought projection methodologies hinges on the integration of the Coupled Model Intercomparison Project Phase 6 (CMIP6 (Meehl et al. 1997; Meehl et al. 2000; Eyring et al. 2016)) models. These models are created by international research institutions, simulate complex interactions within the Earth's climate system and offer projections for future climatic conditions under various emission scenarios. These models can enhance the accuracy of drought projections by considering a range of climatic factors (Cook et al. 2020; Ayugi et al. 2022). This integration facilitates the exploration of uncertainties in climate projections, enabling the design of adaptive strategies to mitigate future drought impacts.

Hence, our analysis revolves around three major research questions: (1) How well do CMIP6 models replicate precipitation patterns across India and its various homogeneous regions during the historical period? (2) What is the future trend of droughts under different emission scenarios? and (3) Why is it so? By achieving these objectives, this study intends to provide valuable insights for informed decision-making, resource management, and climate adaptation strategies in the context of evolving drought patterns in India.

2 | Data and Methods

2.1 | Study Region

India, a vast and geographically diverse country, is characterised by a wide range of climatic, topographic, and ecological conditions. It extends from approximately 5° N to 37° N in latitude and 68° E to 100° E in longitude, covering a landmass of over 3.2 million square kilometres. Given the intricate climatic diversity across India, it becomes essential to adopt a regional approach to comprehensively understand drought dynamics. To achieve this, India has been divided into six homogeneous regions (Sontakke and Singh 1996, 1999), each characterised by relatively similar climatic conditions, geographical features, and ecological settings. All the six homogeneous regions along with their code and domain are represented in Table 1 and the spatial variation can be seen in Figure 1.

TABLE 1 | Six homogeneous regions of India along with their spatial domain and codes used in this study.

Region	Code	Sub-region	Domain	
			Longitude	Latitude
R1	NWI	North western India	72°–79°	21°–30°
R2	NCI	North central India	79°–87°	21°–28°
R3	WPI	West Peninsular India	73°–78°	16°–21°
R4	EPI	East Peninsular India	78°–84°	16°–21°
R5	SoPI	South Peninsular India	75°–80°	10°–16°
R6	NEI	North eastern India	90°–95°	23°–28°

2.2 | Observational Datasets

In this study, we utilise the high-resolution daily gridded rainfall dataset developed by the National Climate Centre (NCC) of the India Meteorological Department (IMD), covering the period 1901–2014 (Pai et al. 2014). The dataset spans the entire Indian subcontinent at a spatial resolution of 0.25° × 0.25° (approximately 625 km^2 per grid cell) and is available at daily temporal intervals. It is constructed using data from more than 6955 quality-controlled rain gauge stations, offering a spatially consistent representation of precipitation across India. Whilst there are known concerns related to temporal inconsistencies in station density and daily reporting frequency, particularly prior to 1981 (Lin and Huybers 2019; Singh et al. 2019), this dataset remains the most comprehensive and reliable observational resource available for long-term hydroclimatic analysis in India. Previous studies (Rajeevan et al. 2008; Roxy et al. 2017; Krishnan et al. 2020) have extensively used this dataset for assessing Indian monsoon variability, validating models, and studying climate extremes. We acknowledge its limitations and advise caution when interpreting trends in extremes, especially over regions with historically sparse station coverage. Nevertheless, the IMD gridded product serves as a valuable reference for model evaluation and historical drought assessment in this study.

2.3 | Model Datasets

In the validation phase aimed at ensuring accuracy, a diverse array of datasets from 10 Coupled Model Intercomparison

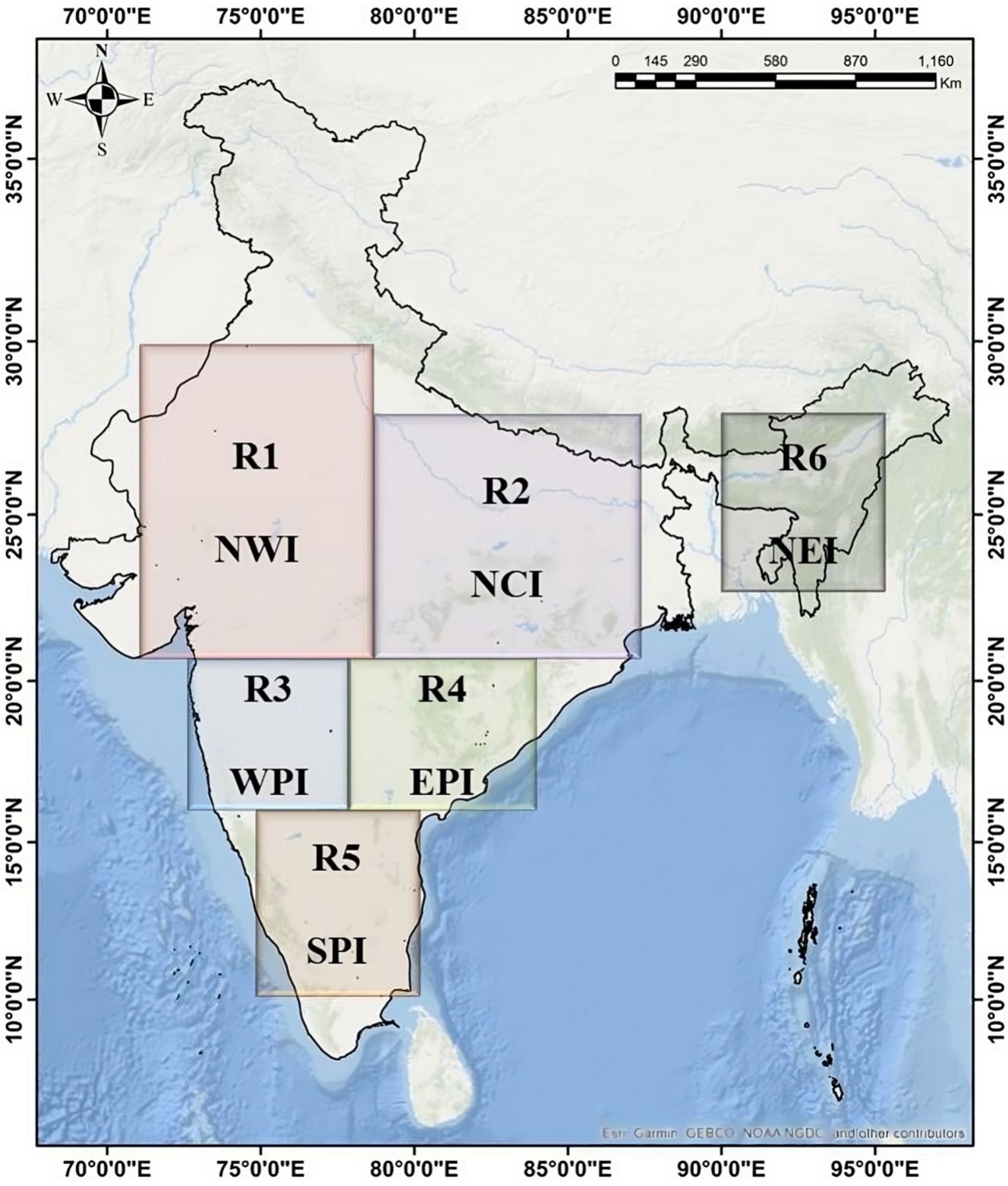

FIGURE 1 | Study region depicting India and its six homogeneous regions. [Colour figure can be viewed at wileyonlinelibrary.com]

Project Phase 6 (CMIP6) as depicted in Table 2 were meticulously chosen (Reddy and Saravanan 2023) for the historical (1901–2014) period. A multimodel ensemble, of all these 10 models has also been employed. Amongst modelling research groups, the Multimodel Ensemble (MME) stands out as the most robust and extensively utilised. So, after all the validation and evaluation, MME is selected for future (2031–2100) time scales for the two future scenarios (Shared Socioeconomic Pathways (SSP) 245 and 585, where SSP245 represents an intermediate "middle of the road" scenario and SSP585 is a high emissions "fossil-fueled development" scenario (O'Neill et al. 2016)). Subsequently, the selected CMIP6 datasets are utilised to calculate Standardised

TABLE 2 | List of CMIP6 models used along with horizontal resolution and institute of origin.

CMIP6 models	Institution	Horizontal resolution	References
ACCESS-CM2	Australian Community Climate and Earth System Simulator- Climate Model 2 Australia	1.9°×1.2°	Bi et al. (2020)
ACCESS-ESM1-5	Australian Community Climate and Earth System Simulator- Earth System Model 1.5 Australia	1.9°×1.2°	Ziehn et al. (2020)
CanESM5	Canadian Center for Climate Modelling and Analysis	2.8°×2.8°	Swart et al. (2019)
IITM-ESM	Indian Institute of Tropical Meteorology	1.1°×1.1°	Krishnan et al. (2019)
MIROC6	Japan Agency for Marine-Earth Science and Technology	1.4°×1.4°	Tatebe et al. (2019)
MPI-ESM1-2-LR	Max Planck Institute for Meteorology, Germany	1.9°×1.9°	Mauritsen et al. (2019)
MPI-ESM1-2-HR	Max Planck Institute for Meteorology, Germany	0.9°×0.9°	Müller et al. (2018)
MRI-ESM2-0	Meteorological Research Institute, Tsukuba, Japan	1.1°×1.1°	Yukimoto et al. (2019)
NorESM2-LM	Norwegian Climate Centre	2.5°×1.9°	Seland et al. (2020)
NorESM2-MM	Norwegian Climate Centre	0.9°×1.3°	Seland et al. (2020)

Precipitation Index (SPI). All these models had significantly different resolution (Table 2), hence, these datasets were bi-linearly interpolated to IMD resolution using Climate Data Operator (CDO).

2.4 | Methodology

2.4.1 | Standardised Precipitation Index (SPI)

In his paper, McKee et al. (1993) stated that the Standardised Precipitation Index (SPI; Hao and AghaKouchak 2013; Wang et al. 2021) stands as a pivotal drought indicator for assessing the likelihood of rainfall occurrence within a specific region over a designated time frame. Its exceptional sensitivity to drought variations makes it a valuable tool across various temporal scales in drought assessments (He et al. 2011; Gocic and Trajkovic 2013; Touma et al. 2015; Farahmand and AghaKouchak 2015; Papalexiou et al. 2021; Dixit and Jayakumar 2022; Verma et al. 2022, 2023). To calculate SPI, long-term precipitation data, that too at multiple time scales, is gathered. This historical precipitation record is fed to a probability distribution function (PDF) so as to transform this distribution into a standard normal distribution, resulting in a mean SPI value of zero for the desired location and timeframe (Edwards and McKee 1997). It can be calculated for various time spans to encompass both short-term (less than 3 months) and long-term droughts (greater than 3 months). In this study, the 3-month time scale is employed to identify drought occurrences, effectively capturing seasonal droughts as outlined by Xu et al. (2015). The SPI values focusing on droughts and their categories can be seen in Table 3.

There are mainly two equations involved in the calculation:

$$P_n^l = \sum_{i=0}^{l-1} \left(P_{n-i}\right), n \geq 1$$

TABLE 3 | Classification of drought based on the SPI index.

Drought category	SPI values
Near normal	−0.49 to 0.49
Mild drought	−0.99 to −0.50
Moderate drought	−1.49 to −1.00
Severe drought	−1.99 to −1.50
Extreme drought	≤−2.0

$$f(P) = \frac{1}{\beta^{\alpha}\Gamma(\alpha)} P^{\alpha-1} e^{\frac{-P}{\beta}}, \alpha, \beta \geq 0$$

where, aggregation timescale in months, n—calculation number, $n \geq l$, $f(P)$—probability distribution function, P—monthly precipitation, $\Gamma(\alpha)$—gamma function, α—shape parameter, β—scale parameter.

2.4.2 | CMIP6 Model Selection

To assess the performance of the model, Taylor's diagram (Taylor 2001) is used to compare the CMIP6 datasets with IMD rainfall data over India. This diagram serves as a comprehensive metric to assess the degree of similarity between our model's predictions and the actual observations. It quantifies key statistical measures, including the correlation coefficient (CC), root-mean-square error (RMSE), and standard deviation (SD), providing insights into the model's performance. The graphical representation on a two-dimensional plot condenses these metrics into a single data point. By analysing this data point, we ascertain the agreement between our model's simulations and the observed data. An ideal model simulation aligns closely with the observation, exhibiting a high CC, low RMSE, and a substantial SD. The mathematical formula for Taylor's diagram used in this process is given as:

$$E'^2 = \sigma_f^2 + \sigma_r^2 + 2\sigma_f \sigma_r R$$

where R—correlation coefficient, E'—RMSE, σ_f and σ_r insights into the model's ability to outperform baseline expectations, emphasising its predictive capabilities. It is m—standard deviation of test and reference datasets.

Secondly, we introduce the Skill Score (SS) as another parameter in our assessment. The skill score offers a nuanced evaluation by measuring the model's performance relative to a reference model or climatological averages. Here a perfect forecast corresponds to the zero value of MSE and 1.0 of SS. This parameter can be mathematically written as:

$$\mathrm{SS} = 1 - \frac{\mathrm{MSE}_{\mathrm{forecast}}}{\mathrm{MSE}_{\mathrm{reference}}}$$

where, MSE—mean squared error, which is calculated as:

$$\mathrm{MSE} = \frac{\sum_{t=1}^{N} E_t^2}{N}$$

Furthermore, Nash-Sutcliffe Efficiency (NSE) is also calculated for all models over different homogeneous regions of India. NSE signifies how well the plot of observed versus model simulated data fits the 1:1 line. It is calculated using the formula;

$$\mathrm{NSE} = 1 - \left[\frac{\sum_{i=1}^{n} \left(X_i^{\mathrm{obs}} - X_i^{\mathrm{model}} \right)^2}{\sum_{i=1}^{n} \left(X_i^{\mathrm{obs}} - X^{\mathrm{mean}} \right)^2} \right]$$

These parameters are computed for all the 10 CMIP6 models and MME for the historical period (1901–2014). Further, Figure 2 represents the complete methodology adapted in this study.

3 | Results and Discussion

3.1 | Spatial Assessment for Historical Period

Figure 3 presents a spatial plot delineating the accumulated precipitation patterns during the Indian summer monsoon seasons, spanning from June to September (JJAS) across the six homogeneous regions of India, for the historical period (1901–2014). This depiction incorporates observational data from the IMD alongside simulations from 10 distinct CMIP6 models and their MME (Soni et al. 2023; Konda and Vissa 2023; Reddy and Saravanan 2023). Upon detailed inspection, it is apparent that the IMD observational data closely mirrors the precipitation patterns of MPI-ESM-1-2-HR and Nor-ESM-MM within the NEI region. Furthermore, MPI-ESM-1-2-LR exhibits similarities with the observed precipitation pattern (Kumar and Sarthi 2021), although with some notable distinctions. In the NCI region, a similar alignment is observed between IMD observations and the aforementioned models. Moving to the EPI region, we observe that IMD observations and CMIP6 models, particularly MPI-ESM-1-2-HR, MIROC6 and MME, share a considerable resemblance in accumulated precipitation patterns. In contrast, the SoPI region showcases convergence between IMD observations and models, including MRI-ESM, CanESM5, ACCESS-CM and MME. In the NWI region, the observed accumulated precipitation aligns closely with MPI-ESM-1-2-HR, indicating strong fidelity in representing precipitation dynamics. However, it is important to note that variations in spatial patterns become apparent in certain regions, such as NWI, NCI and EPI, when considering models like CanESM5 and ACCESS-ESM-12. To further accentuate the closeness, it becomes mandatory to examine model precipitation bias (Figure 4).

Notably, in Figure 4, it is highlighted that MPI-ESM-1-2-HR, MPI-ESM-1-2-LR, and Nor-ESM-MM stand out with remarkably reduced bias compared to other models. Subsequently, relatively minor biases are exhibited by MME and MPI-ESM-LR, whereas the most significant biases amongst the six homogeneous regions are indicated by the ACCESS-ESM-15 model. Following ACCESS-ESM-15, varying degrees of bias are observed in CanESM5, ACCESS-CM, NorESM-LM, IITM-ESM, MRI-ESM-20, MIROC6, and NorESM-MM. Significantly, greater negative biases are observed with the Can-ESM5 model, over most of the regions including NWI, NCI, and EPI, and by IITM-ESM and CAN-ESM models over NEI. These biases depict deviations ranging from −6 to −10. Similarly, more positive biases are indicated over peninsular regions (WPI, EPI and SoPI), whilst significant negative biases exceeding −4 are evident over NWI by MIROC6. Amongst the 10 models assessed, the most substantial biases are associated with ACCESS-ESM-15, CanESM5, and ACCESS-CM, whilst the least pronounced biases are exhibited by MPI-ESM-LR, MPI-ESM-HR, Nor-ESM-MM models, and MME. It is important to note that spatial pattern variations are observed within different regions. This underscores the critical necessity for region-specific assessments and fair model selection.

3.2 | Drought Assessment Through SPI

Drought monitoring based on SPI-3 from different CMIP6 models is compared with IMD data for studying long-term drought characteristics. The SPI timeseries estimated over all India regions for the historical period of 1901–2014 are shown in Figure 5. The time series plots of the index indicate the significant drought events that occurred in this period, matching quite well with the major drought years such as 1901, 1904, 1905, 1907, 1911, 1913, 1915, 1918, 1920, 1925, 1939, 1941, 1951, 1965, 1966, 1968, 1972, 1974, 1979, 1982, 1985, 1987, 2002, 2004, and 2009 identified by the IMD, characterised as moderate to severe drought years. Figure 5b shows that models: MPI-ESM-12-LR, MPI-ESM-12-HR, MRI-ESM-20, NorESM2-LM, NorESM2-MM, and MME exhibit a notably accurate detection of drought episodes during the years 1907, 1913, 1918, 1920, 1965, 1966, 1972, 1979, 1982, 1986, 1987, 2002, 2004, 2009, and 2014 (Verma et al. 2023), corroborated by RegCM 4.7 (Bhatla et al. 2019, 2020). Therefore, it is reasonable to conclude that the model estimations improved in precision for later years. On the other hand, CAN-ESM5 and MPI-ESM 1.2-LR initially demonstrated accurate predictions, but their forecasting accuracy waned towards the end of the decade.

Going into regional details, SPI value showed that within the SoPI region, the years 2011, 2007, and 2001–2006 point to extended periods of severe drought. During the drought

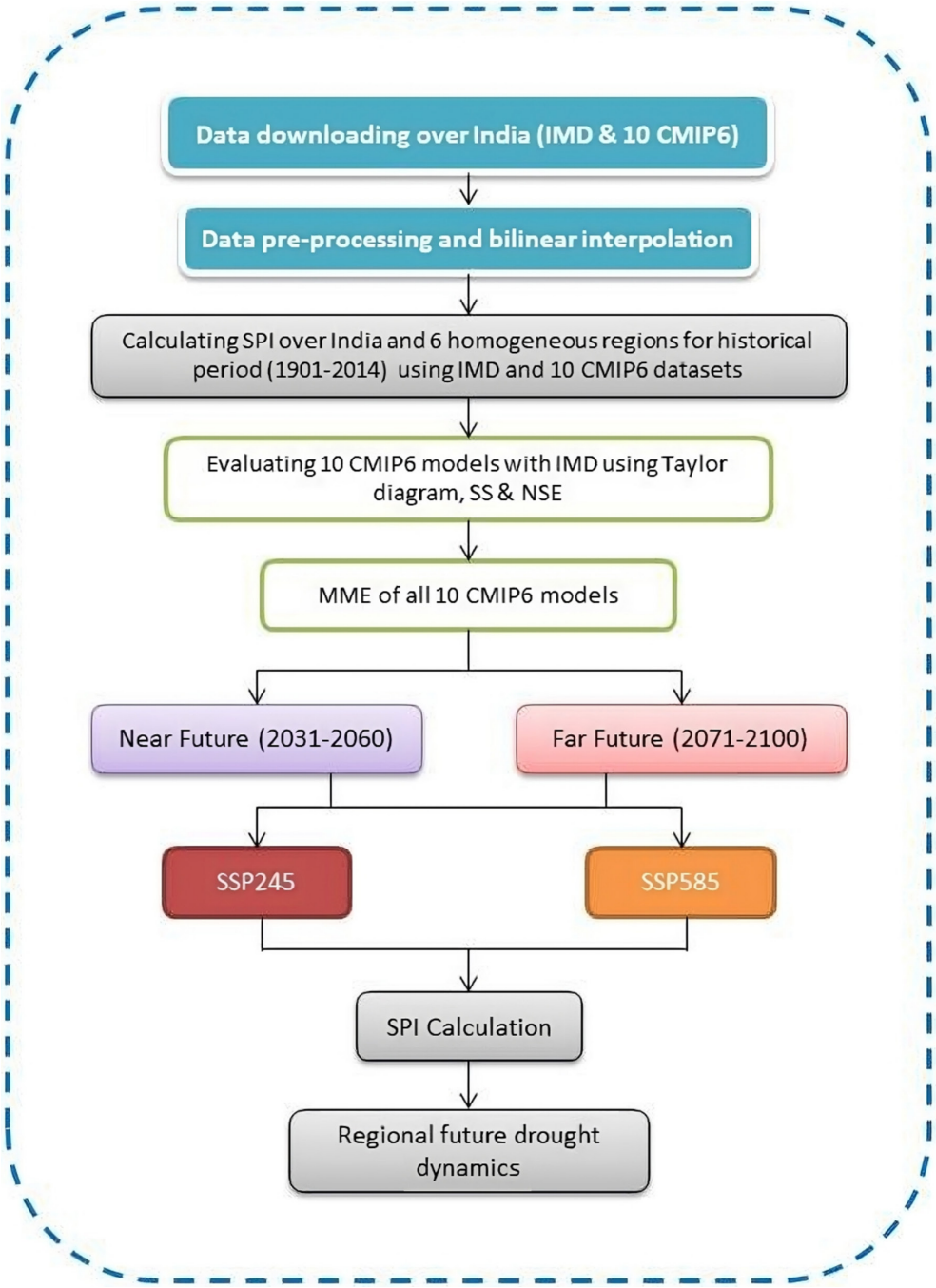

FIGURE 2 | Flow chart representing detailed methodology adapted in this study. [Colour figure can be viewed at wileyonlinelibrary.com]

years, IMD's SPI values align with specific models, including ACCESS-CM, CanESM5, IITM-ESM, MPI-ESM-12-LR, MPI-ESM-12-HR, MRI-ESM-20, NorESM2-LM, NorESM2-MM and MME, showcasing their ability to capture dry conditions. In contrast, ACCESS-ESM15 and MIROC6 often represented wet conditions during these years. Also, over the NWI region, models such as ACCESS_CM2, ACCESS_ESM15, NorESM2_MM, NorESM2_LM, MRI-ESM-20, MPI-ESM_1–2-HR, MPI-ESM_1–2-LR, MIROC6 and MME performed quite well. However, certain models like IITM-ESM and others occasionally presented opposite wet conditions or divergent patterns compared to the IMD observations. Analysing the EPI region, IMD data reveals a consistent pattern of dry or drought years in 1902, 1904, 1952, 1956, 1966, 1967, 1968, 1971, 1972, 1973, 1987, 2002, and 2012, with alignment to various models. These models include NorESM2-MM, MPI-ESM-20, MPI-ESM-1-2-HR, CanESM5, IITM-ESM, MIROC6 and MME. Conversely, wet conditions are observed in these years with models like Nor-ESM2-MM, MPI-ESM-1-2-LR, ACCESS-CM2, and ACCESS-ESM-15. Additionally, the years 1936, 1959, 1971, and 1973 depict wet conditions as suggested by IMD data, whilst dry years are indicated by models IITM-ESM, MIROC6, MPI-ESM-1-2-LR, CanESM5, ACCESS-ESM15, MPI-ESM-1-2-HR, MRI-ESM20, NorESM2-MM, and NorESM2-LM. In 2014, IMD data corresponds with dry conditions, which are well mirrored by CanESM5, IITM-ESM, MIROC6, MPI-ESM-1-2-LR, MPI-ESM-1-2-HR, MRI-ESM20, NorESM2-LM, and NorESM2-MM. In contrast,

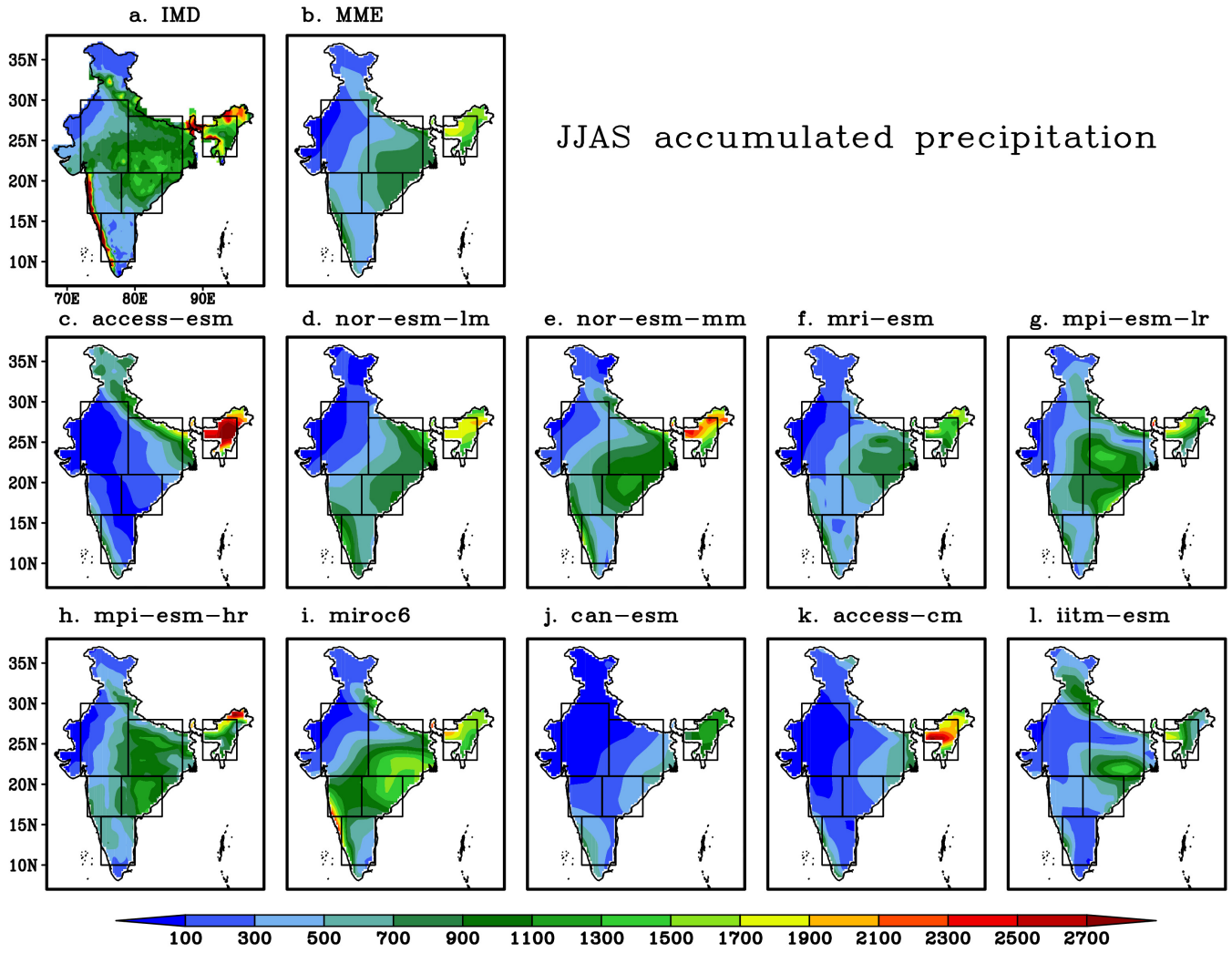

FIGURE 3 | Spatial distribution of accumulated precipitation (in mm) during the monsoon season (JJAS) for 1901–2014 from (a) IMD observational precipitation, (b) MME and 10 CMIP6 GCMs simulated model outputs (c–l) with each box representing different homogeneous regions of India. [Colour figure can be viewed at wileyonlinelibrary.com]

ACCESS-CM2 and ACCESS-ESM-15 exhibit wet conditions for the same year. Furthermore, in the NCI region, dry conditions in 1929, 1987, 2000, 2002, 2009, and 2014 correspond to IITM-ESM, ACCESS-CM, MPI-ESM-12-HR, and more. Whereas, over the WPI region, between 2002 and 2014, IMD SPI data consistently indicated drought conditions aligning with ACCESS-ESM, CanESM5, MPI-ESM-12-HR, MME and NorESM2-MM, whilst contrasting wet conditions are suggested by ACCESS-CM, IITM-ESM, MIROC6, and MPI-ESM-12-LR. A similar pattern emerged in 1998, 1999, and 2000. So, to authenticate the analysis, various statistical parameters have been calculated for the historical period.

3.3 | Statistical Analysis for Model Selection

Figure 6 presents a Taylor diagram (Taylor 2001) that summarises the aggregated statistics for precipitation. In the AI region, MME and ACCESS-ESM models exhibited the highest CC values, approximately 0.79 and 0.72, respectively. They also achieved SS of 0.78 and 0.52, respectively, as indicated in Table 4. Moreover, their SD values closely matched the observations, as shown in Figure 6a. However, it is noteworthy that the NSE values for these models were not particularly favourable. Conversely, ACCESS-CM displayed a CC of 0.64, but its SD values deviated significantly from the observed data, resulting in no significant SS and NSE. Notably, MME, MPI-ESM1-2-LR, MPI-ESM1-2-HR, and NorESM2-MM models demonstrated strong performance when considering SS and NSE. Similarly, in the NWI region, ACCESS-ESM1-5 shows a positive CC of 0.44, indicating an average correlation with observations. However, it has a considerably negative NSE of −6.29 and a slightly negative SS of −1.47, suggesting that it struggles with overall model efficiency. Conversely, ACCESS-CM2 exhibits a lower but still positive CC of 0.22, an NSE of −4.48, and a SS of −1.71, indicating similar challenges in predicting this region's climate patterns. Amongst the other models, like CanESM5 and MPI-ESM1-2-LR, exhibit negative CC, NSE, and SS, indicating poor performance in this region. For NCI, MME stands out with a relatively high CC of

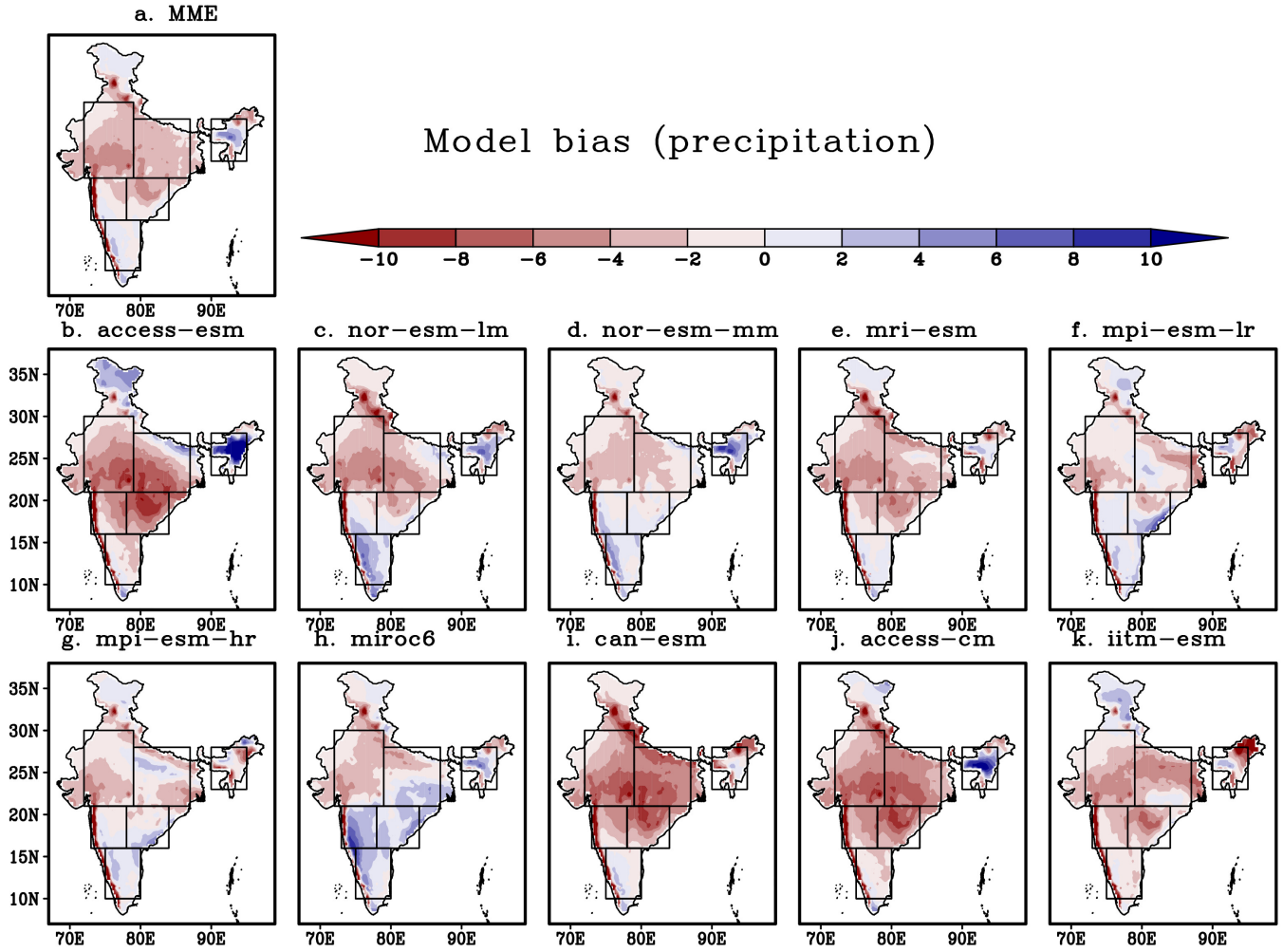

FIGURE 4 | The spatial distributions of MME and each CMIP6 model bias for precipitation during the monsoon season (JJAS) for the historical period (model simulated data—observational data) over India. [Colour figure can be viewed at wileyonlinelibrary.com]

0.70, suggesting a good correlation with the observed data. It also shows a positive SS of 0.68, albeit with a slightly negative NSE of −0.33. MPI-ESM1-2-HR also scores remarkably well in this region, with a high CC of 0.66 and a positive SS of 0.58, indicating its proficiency in modelling. Other models, like ACCESS-CM2, exhibit a positive CC of 0.39 with a lower NSE of −3.84 and a slightly positive SS of −1.42, signifying acceptable but not outstanding performance. In contrast, CanESM5, IITM-ESM, and NorESM2-LM display significant negative CC, NSE, and SS values, indicating inadequate modelling for this region. MME takes the lead in WPI with a CC of 0.77, showcasing a good correlation with the observed climate data. It maintains an NSE of −0.36 and a SS of 0.74. ACCESS-CM2 follows with a CC of 0.20, an NSE of −2.17, and a SS of −0.25, indicating reasonable performance but room for enhancement. Amongst others, MPI-ESM1-2-HR demonstrates a poor CC of 0.30 and a positive SS of 0.28. Furthermore, in the EPI region, most models, including ACCESS-CM2, ACCESS-ESM1-5, and MPI-ESM1-2-HR, display positive CC, NSE, and SS values, indicating their competence in representing the regional climate. ACCESS-CM2 has a CC of 0.34, a slightly negative NSE of −2.92, and a SS of −0.23. MME performs well with a CC of 0.55 and a slightly negative NSE of −0.54, resulting in a SS of 0.79. Over the SoPI region also, MME exhibits promising CC values above 0.7 and positive SS, suggesting reliable regional climate modelling. Lastly, in the NEI region, most models maintain positive CC, NSE, and SS values.

The comparison of the proximity of these models to the observed data based on all these parameters revealed that the ranking of predictive performance was as follows: MME > MPI-ESM1-2-HR > NorESM2-LM > MPI-ESM 1–2-LR > ACCESS-ESM1-5 > NorESM2-MM > MRI-ESM2-0 > MIROC6 > CanESM5 > ACCESS-CM2 > IITM-ESM. Hence, for further analysis, MME is considered for better understanding the trend and dynamics of drought under the two distinct future scenarios, SSP245 and SSP585.

3.4 | Drought Projections

For further investigation, the estimation of drought events using the SPI during the ISM season in NF (2031–2060) and FF (2071–2100) time slices under SSP245 and SSP585 has been done (Figure 7). The analysis reveals notable occurrences of severe and moderate drought events across different regions.

Under SSP245 for the NF, the projections reveal unique drought patterns. Severe drought events are projected in various regions, with the years 2040, 2043, 2044, 2048, 2051, and 2054 identified as critical periods. Additionally, moderate drought events are anticipated in the years 2031, 2038, 2040, 2043, 2047, 2048, 2050, 2051, 2054, and 2059. The AI region

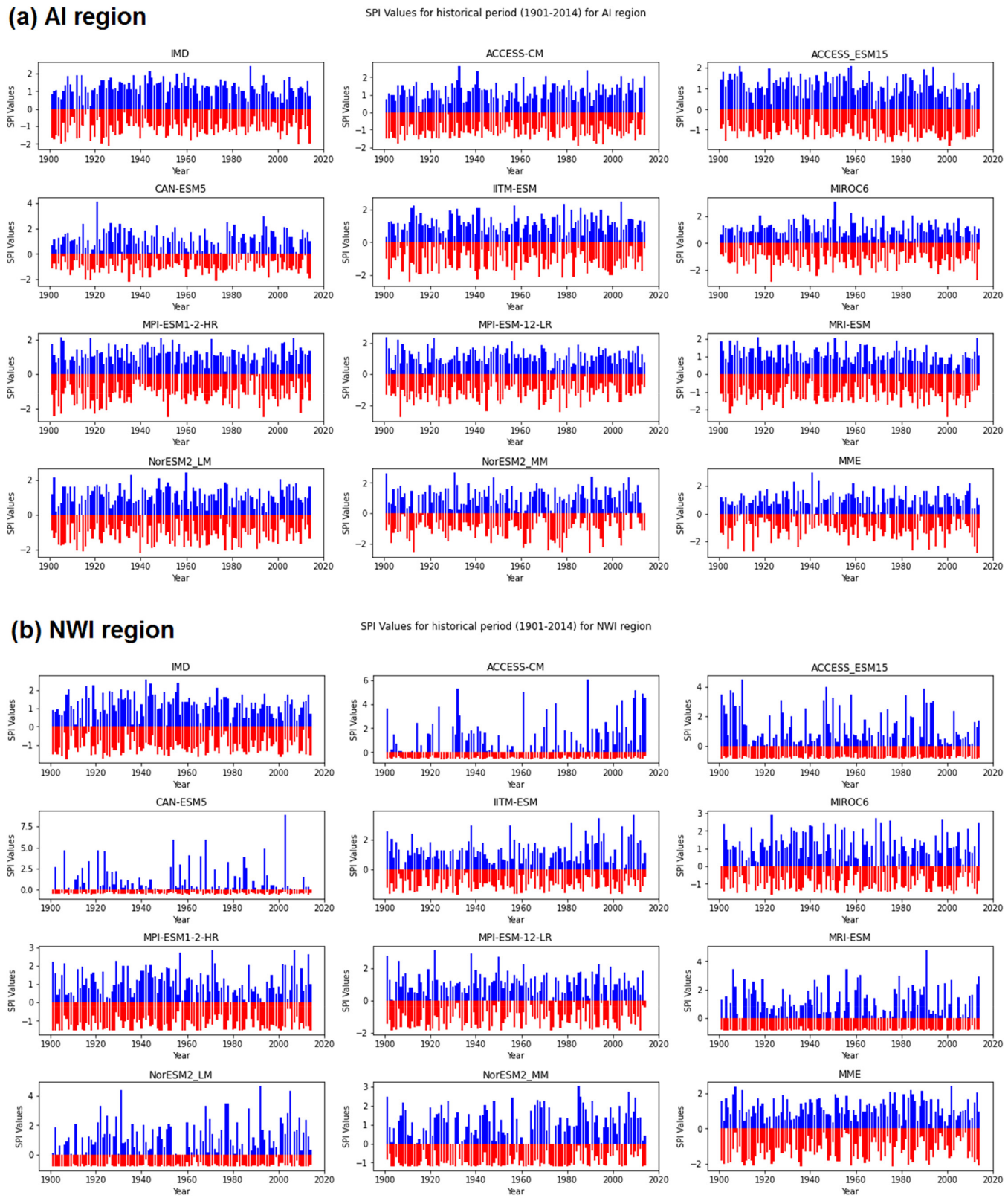

FIGURE 5 | SPI value corresponding IMD, 10 CMIP6 models and MME over (a) India (b) NWI (c) NCI (d) EPI (e) SoPI (f) WPI (g) NEI regions for the historical period (1901–2014) with blue lines showing positive and red lines showing negative SPI values. [Colour figure can be viewed at wileyonlinelibrary.com]

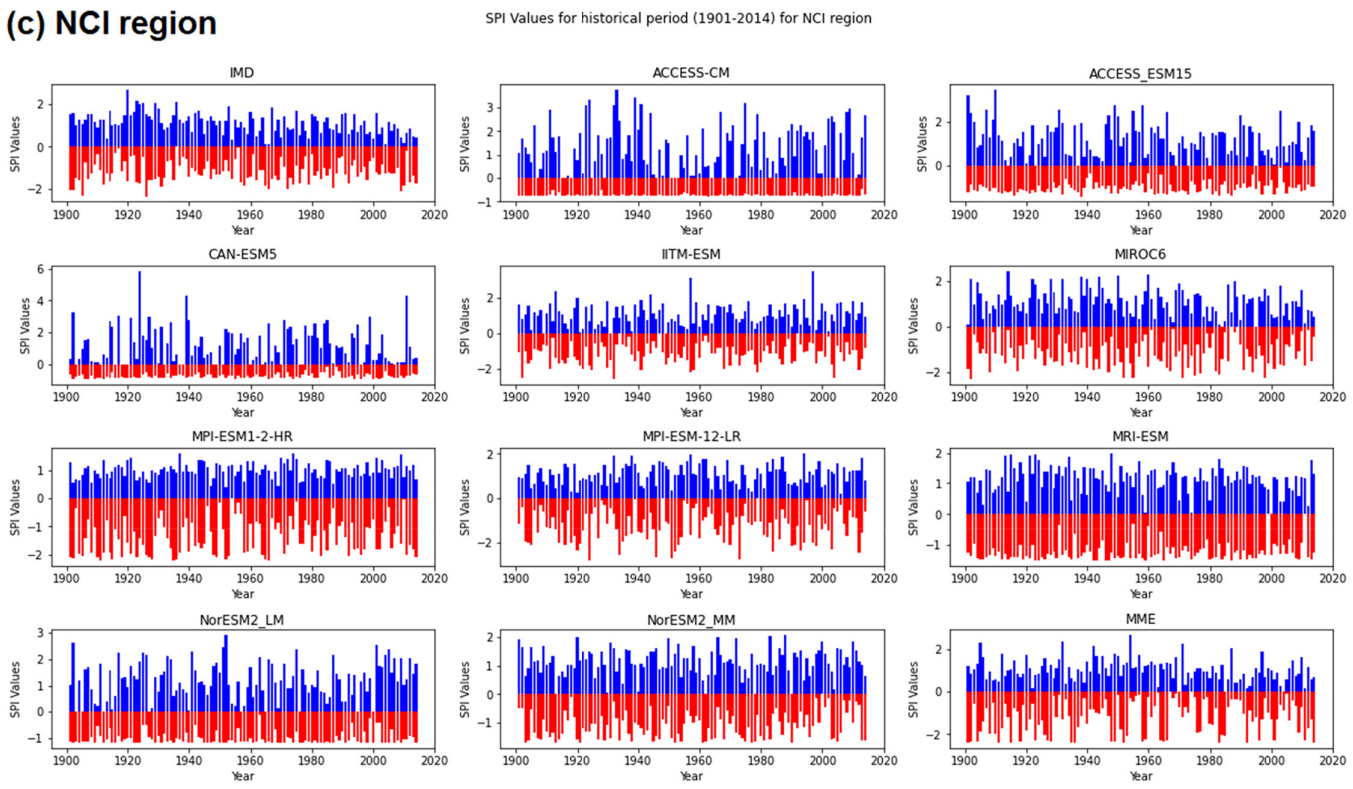

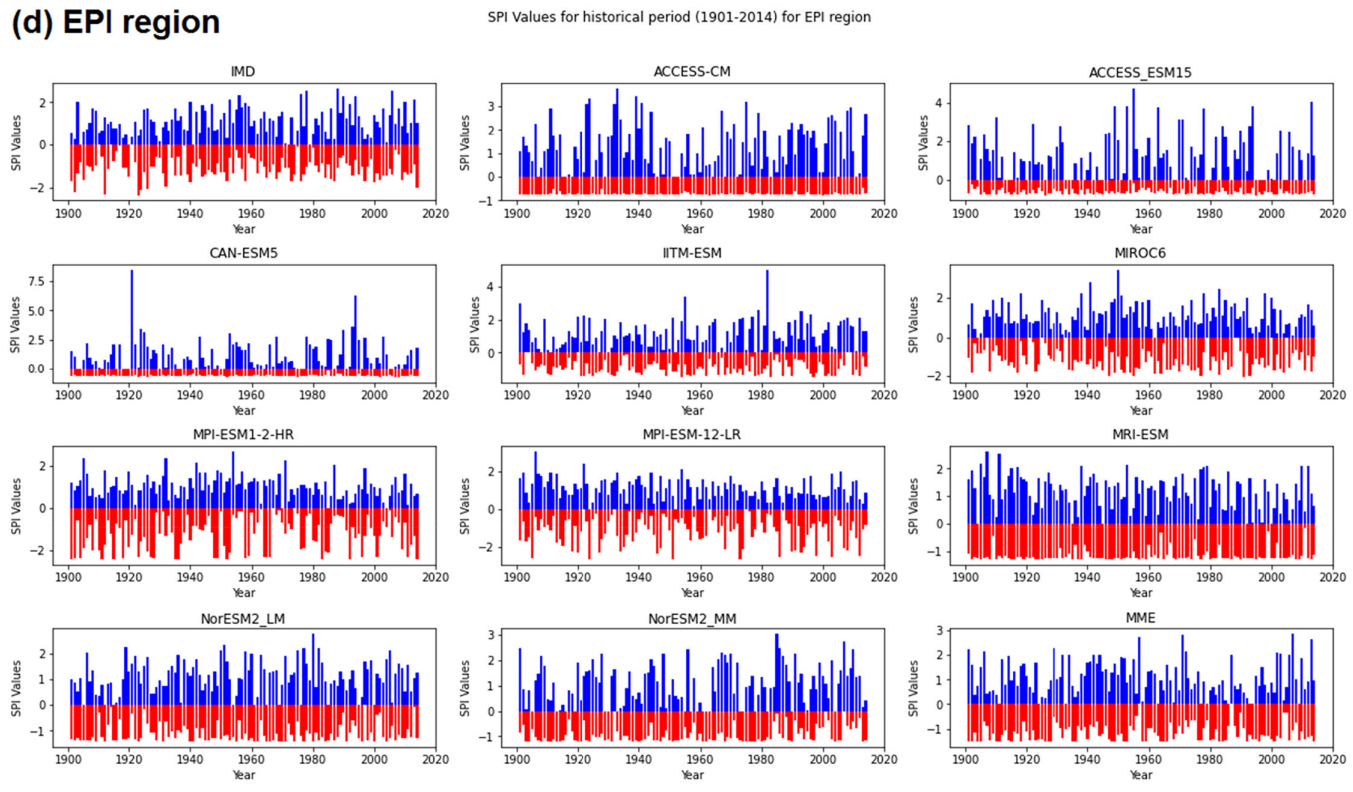

FIGURE 5 | (Continued)

anticipates extreme drought in 2041 and severe events in 2034, 2035, 2037, and 2048. Whereas, EPI foresees extreme drought events in 2042 and 2059, severe events in 2043, 2048, 2059, and moderate events in other years. NCI and NEI regions anticipate extreme drought events in 2031, 2042, and 2059, with severe events in 2042, 2048, 2059, and moderate events in other years. NWI expects extreme drought in 2032, with severe events in 2032, 2041, 2042, 2043, and moderate events in other years. The SoPI region foresees extreme drought events in 2034, 2035, 2042, and 2059, severe events in 2035, 2042, 2043, 2048, and moderate events in other years. WPI envisions extreme drought events in 2042, severe events in 2031, 2042,

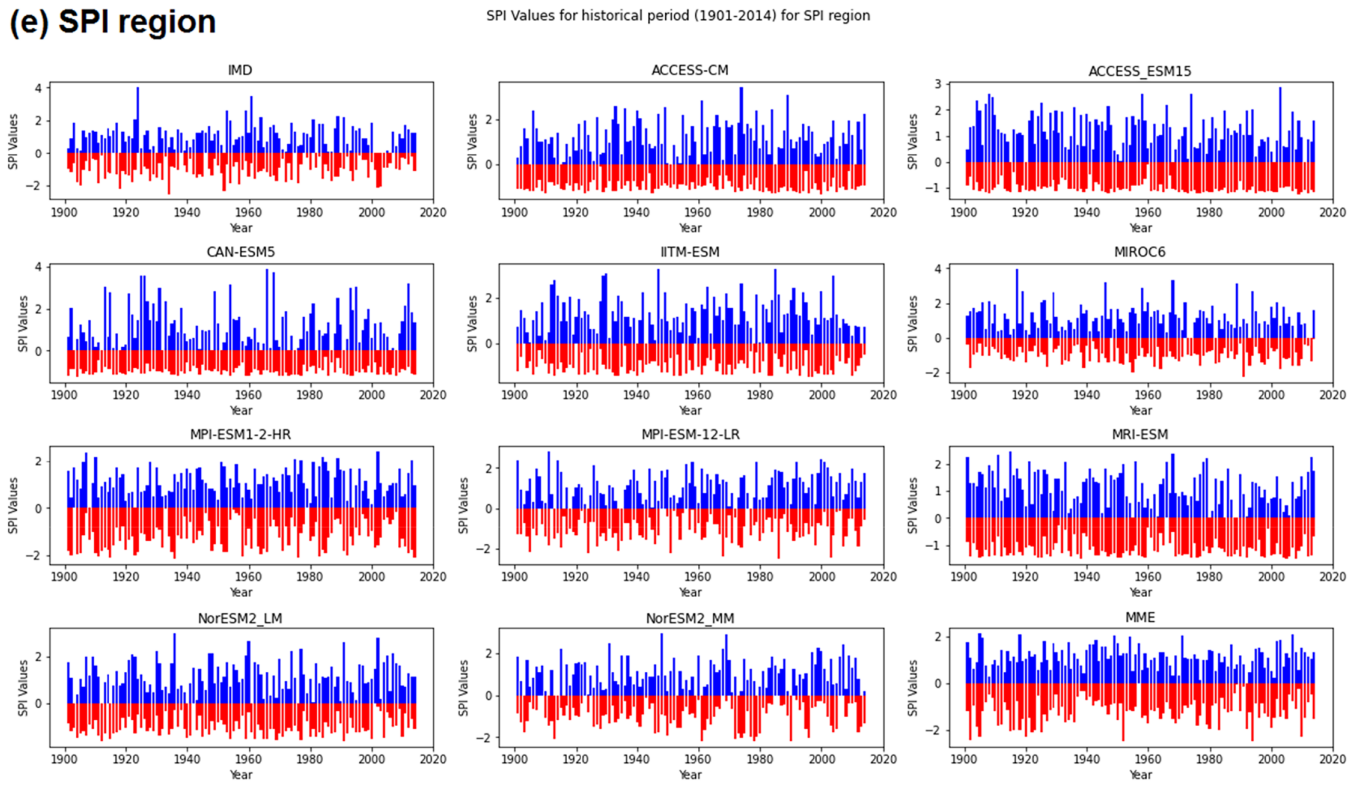

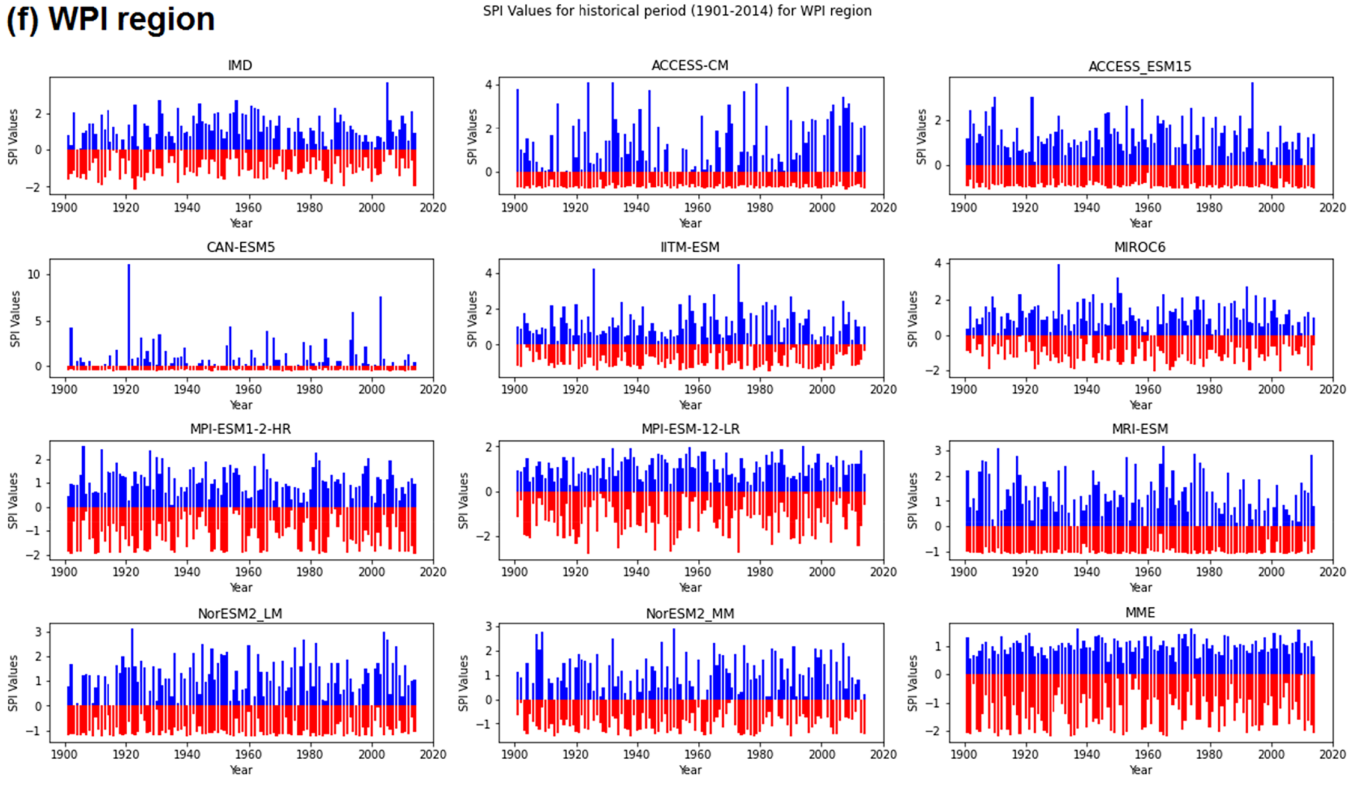

FIGURE 5 | (Continued)

2050, and 2059, and moderate events in other years. Extending the analysis to the FF (Figure 7B1–B7), severe drought events continue in the years 2040, 2042, 2043, and 2054, with 2059 displaying extreme conditions in the NCI region. The EPI region experiences severe drought in 2041, 2042, and 2048, along with an extreme event in 2042. The NEI region faces extreme drought in 2047, accompanied by severe conditions in 2047 and 2054. In the NWI region, extreme drought events in 2040, 2044, and 2054 persist, whilst severe events are observed in 2040, 2041, 2044, and 2048. The SoPI and WPI

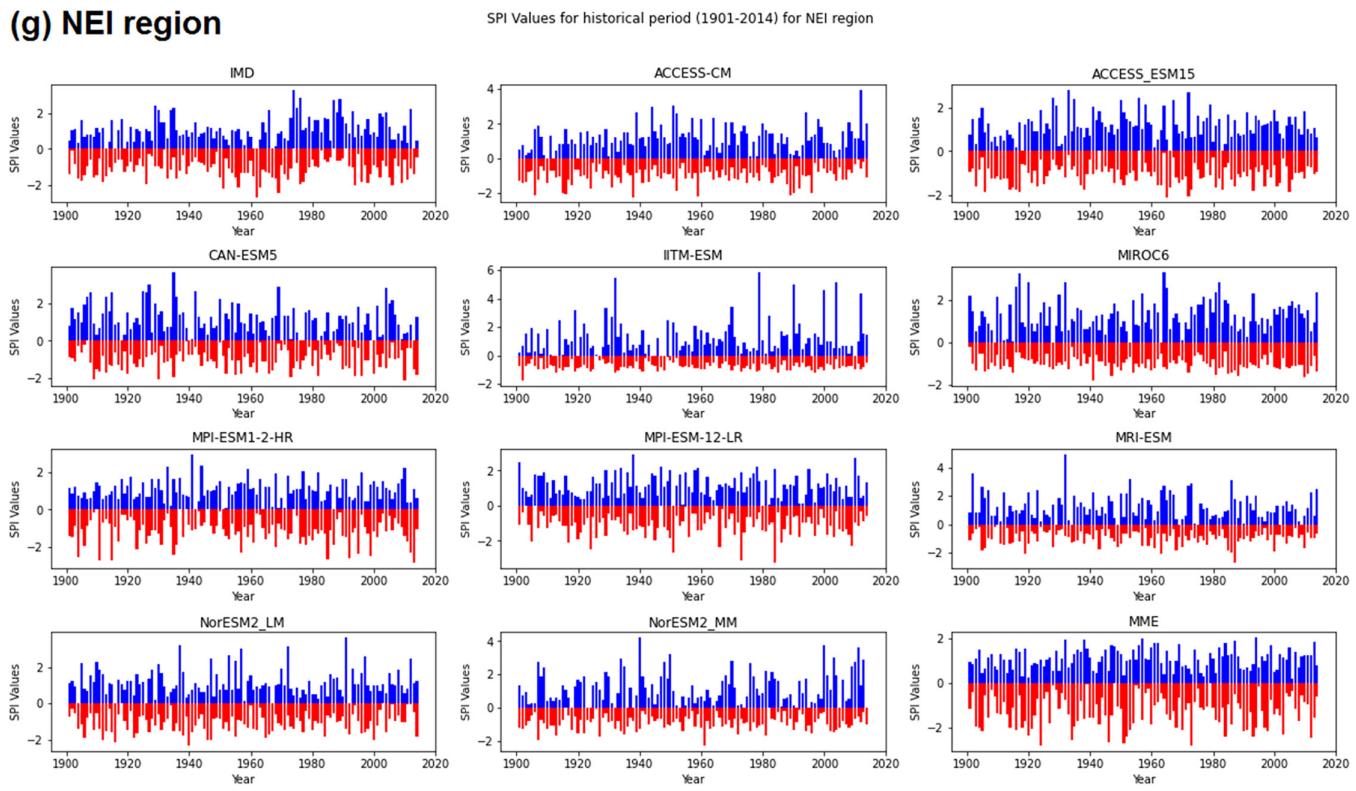

FIGURE 5 | (Continued)

regions encounter severe and extreme drought events in various years. The AI region experiences extreme drought in 2031 and 2043, with severe events in 2031, 2042, and 2044.

Transitioning to SSP585 (Figure 7C1–C7) amplifies the drought challenges, particularly in the NWI region. In the NF period, the years 2044 and 2054 project extreme drought events, whilst 2040, 2043, 2044, and 2048 experience severe conditions. WPI envisions extreme drought in 2044, severe events in 2040, 2043, 2044, and 2048, and moderate events in other years. For the AI region, extreme drought events are anticipated in 2031 and 2043, with severe events in 2031, 2042, and 2044, along with moderate events in other years. Lastly, moving to the FF, across AI, extreme drought events are expected in 2075 and 2098, severe events in 2072, 2074, and 2082, and moderate events in other years. EPI foresees extreme drought events in 2072 and 2075, severe events in 2082, 2083, 2085, and moderate events in other years. NCI anticipates extreme drought events in 2075 and 2089, severe events in 2075, 2078, 2085, and 2089. NWI expects extreme drought in 2074 and 2075, severe events in 2072, 2078, 2082, and moderate events in other years. The SoPI region foresees extreme drought events in 2087 and 2097, severe events in 2074 and 2098, and moderate events in other years. WPI envisions extreme drought events in 2075 and 2089, severe events in 2072, 2073, 2075, 2088, 2089, and 2095, and 2098 (Figure 7D1–D7).

The occurrence of extreme drought events across various regions of India, including AI, EPI, WPI, EPI, SoPI and NCI, indicates an upward trend in frequency as we progress from the NF to the FF as depicted in Figure 8b. This trend holds true for both the SSP245 and SSP585 scenarios in some regions. However, in the NWI and AI regions, there is a notable reduction in extreme drought events from NF to FF, as observed in both scenarios. In the SoPI region, there is a decrease in extreme drought events from NF to FF under the SSP245 scenario, whilst an increase in extreme drought events is projected under SSP585. In the NEI region, the frequency of moderate drought events remains relatively stable under SSP245, whilst a decrease is anticipated under SSP585. Furthermore, concerning severe drought events across India, there is an overall increase in frequency under both SSP245 and SSP585. However, in the EPI region, there is a likelihood of a decrease in the frequency of severe drought events under both SSP scenarios. In the NCI and WPI regions, severe drought events are projected to decrease. Conversely, the NWI, NCI and WPI regions are expected to experience an increase, and the NWI and SoPI regions may experience a decrease under the SSP585 scenario. The SoPI region under the SSP245 scenario may maintain a similar frequency of severe drought events from NF to FF. In the NEI region, the frequency of severe drought events is anticipated to remain relatively constant under both SSP245 and SSP585. Also, the distribution of these SPI values over different regions is given by box plot as depicted in Figure 9.

In the WPI, NCI, and NWI regions, the box plots reveal that the most severe drought conditions, represented by the minimum (lowest whisker), occur in the FF under SSP585. This suggests a substantial increase in drought intensity in these regions. On the other hand, the NEI region experiences the highest SPI values in NF under SSP585, indicating a different temporal pattern and implying more immediate changes in drought conditions in this region. For the SoPI and EPI regions, the highest values are found in NF under SSP245. These regions also exhibit a

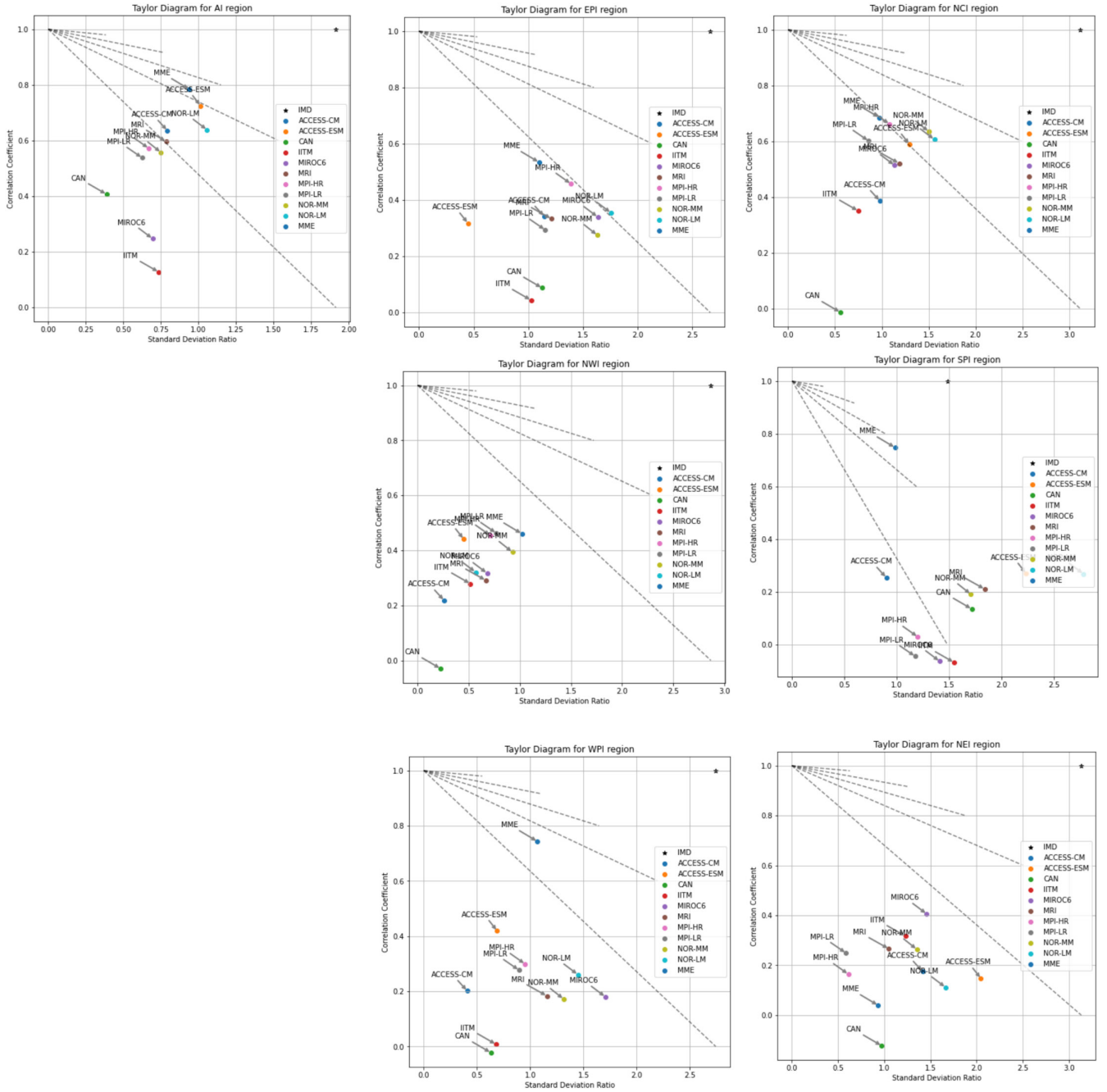

FIGURE 6 | Taylor diagram representing CC and SD over India and its six homogeneous regions, with each distinct coloured sphere representing different CMIP6 model datasets. IMD data is set as a reference point and represented by a star at the top right corner. [Colour figure can be viewed at wileyonlinelibrary.com]

more extensive distribution of data, suggesting not only higher drought intensity but also a potential for longer-lasting impacts during the near future under the SSP245 scenario. Furthermore, the interquartile range (IQR), which represents the spread of the data within the box of the box plot, shows considerable variation. Specifically, the WPI and NCI regions exhibit the maximum IQR in the FF under SSP585, indicating a wider range of drought intensity values during this period in these regions. To gain insight into the cause behind these statistics, it is necessary to investigate the dynamics involved.

The spatial plot of precipitation offers a critical perspective on the evolving atmospheric dynamics within our study regions (Figure 10a–f). Notable variations in rainfall patterns can be seen that are crucial in comprehending future drought scenarios. It is evident that certain regions experience a decline in precipitation, potentially increasing their susceptibility to drought. In contrast, other areas display variations in the intensity and frequency of rainfall, which could have distinct implications for local hydrological systems and agricultural practises. In the context of SSP245, for NF, it is clear that the SoPI region receives precipitation of about 3–5 mm/day, whilst the WPI regions exhibit 3–7 mm/day. In the EPI regions, the eastern part gets 7–9 mm/day, and the NEI regions show variation, with the northern part receiving 13–15 mm/day. The NWI region varies from 1 to 7 mm/day. More intensified

TABLE 4 | Statistical indicators of precipitation GCMs CMIP6 models using SS and NSE.

Models	AI		NWI		NCI		WPI		EPI		SPI		NEI	
	SS	NSE	SS	NSE	SS	NSE	SS	NSE	SS	NSE	SS	NSE	SS	NSE
ACCESS-CM2	−0.17	−2.64	−1.71	−4.48	−1.42	−3.84	−0.25	−2.17	−0.23	−2.92	−2.18	−3.25	−1.16	−2.20
ACCESS-ESM1-5	0.44	−0.72	−1.47	−6.29	0.04	−0.91	−2.12	−0.15	−0.27	−1.95	−0.92	−0.27	−1.21	−0.42
CanESM5	−0.39	−2.41	−2.17	−5.39	−1.53	−5.21	−1.33	−0.12	−0.19	−3.06	−1.11	−0.14	−2.05	−0.02
IITM-ESM	0.00	−0.13	−0.83	−2.66	0.20	−0.56	−0.57	−0.32	0.03	−0.92	−1.20	−0.07	−1.00	−0.01
MIROC6	0.27	−0.25	−0.40	−2.00	0.43	−0.13	0.00	−0.41	0.18	−0.59	−0.55	−0.06	−0.80	−0.18
MPI-ESM1-2-LR	0.27	−0.60	−0.68	−2.40	−0.03	−1.06	−0.23	−0.27	−0.32	−1.74	−0.74	−0.21	−1.00	−0.18
MPI-ESM1-2-HR	0.51	−0.57	0.06	−0.87	0.58	−0.16	0.05	−0.16	0.23	−0.48	−0.44	−0.03	−0.02	−0.30
MRI-ESM2-0	0.48	−0.54	0.15	−0.69	0.59	−0.21	−0.08	−0.25	0.43	−0.08	−0.27	−0.04	0.01	−0.28
NorESM2-MM	0.55	−0.56	−0.30	−1.77	0.27	−0.37	−0.06	−0.26	0.15	−0.70	−0.65	−0.19	−0.33	−0.17
NorESM2-LM	0.52	−0.64	−0.37	−2.00	−0.13	−1.32	−0.55	−0.11	−0.36	−1.97	−1.35	−0.27	−0.51	−0.26
MME	0.78	−0.57	0.73	−0.41	0.68	−0.33	0.74	−0.36	0.79	−0.54	0.74	−0.48	0.80	−0.61

values of precipitation can be observed over NWI and some parts of the NCI region for the FF time slice. More positive changes are identified in the NWI and EPI regions, (ranging from 2 to 3.5). In the NEI region, these positive changes extend to Nagaland and its neighbouring areas. Conversely, intensified negative changes are pronounced over the WPI and some parts of the NCI region.

The observed trends in precipitation changes across various regions of India can be attributed to a combination of atmospheric physics and climatic factors. The increase in precipitation over parts of India, particularly in regions like Madhya Pradesh, can be associated with the physics of a warming atmosphere. Warmer air has a higher capacity to hold moisture, following the Clausius–Clapeyron relation, which states that for every degree Celsius of temperature increase, the atmosphere's water-holding capacity increases by about 7% (Trenberth 1999). This means that in a warmer climate, the atmosphere can contain more water vapour, potentially leading to increased precipitation. On the other hand, regions experiencing decreased precipitation, such as the Western Ghats and parts of Karnataka and Maharashtra, may be influenced by changes in atmospheric circulation patterns. Furthermore, the impact of these changes can vary between the two emission scenarios, SSP245 and SSP585. The higher emission scenario, SSP585, leads to more pronounced warming, increasing the atmospheric water-holding capacity further and potentially intensifying the monsoon system. In contrast, the lower emission scenario, SSP245, might not produce as substantial warming and may even lead to changes in atmospheric circulation patterns that reduce moisture transport to specific regions, resulting in decreased precipitation (Held and Soden 2006) as justified in Figure 11a–f.

During the NF under SSP245, the MSLP variations are indicative of regional pressure systems that influence monsoon precipitation. The relatively lower MSLP in the NCI region (Figure 10g–l) (around 998–1002 hPa) suggests the presence of a low-pressure system, which tends to draw in moist air from the surrounding regions. This, in turn, fosters increased monsoon precipitation in this area as justified in Figure 10a–f. Conversely, the higher MSLP in the SPI region (around 1008–1010 hPa) is associated with descending air masses, leading to relatively lower precipitation; hence, dry conditions. For the FF time slice, the MSLP patterns exhibit similarities to the NF, indicating the persistence of these pressure systems (Wang et al. 2001). The MSLP distribution in the NWI region continues to influence precipitation (Krishnamurti and Bhalme 1976), experiencing comparatively greater MSLP and decreased precipitation. The changes (FF-NF) can also be linked to altered pressure gradients and associated wind patterns, which impact the monsoon circulation (Xie et al. 2010). In the NWI and WPI regions, where MSLP increases by 0.1–0.3 hPa, there is an indication of strengthening high-pressure systems. This can result in reduced convergence of moist air, potentially leading to decreased precipitation; hence, possible drought conditions. The northern part of NWI maintains higher values, promoting decreased precipitation.

These results can be further validated by looking into the prevailing patterns of relative humidity (Figure 10m–r). Under the

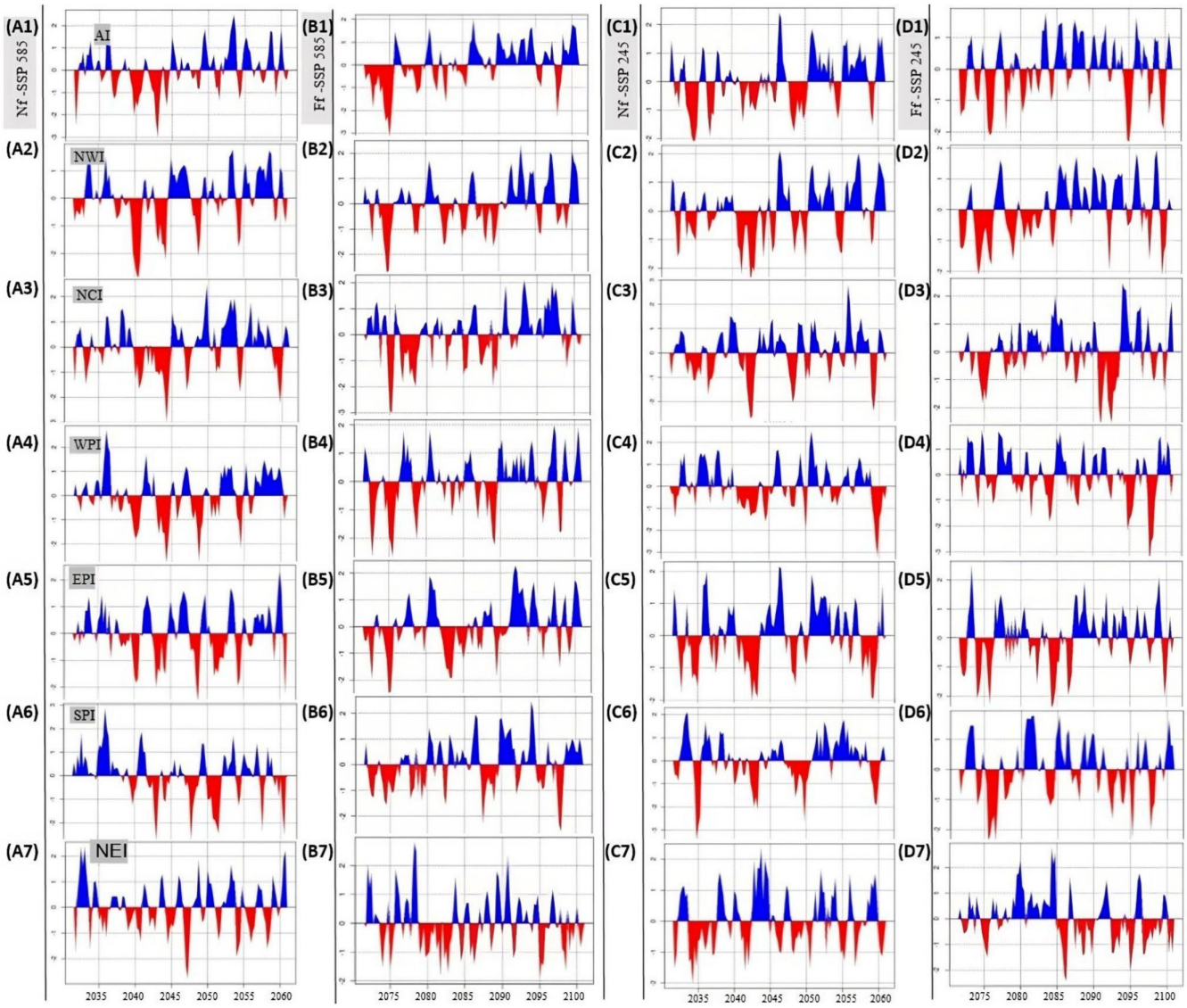

FIGURE 7 | SPI value over India and its distinct homogeneous regions (A1-A7), (C1–C7) during NF (2031–2060) and (B1–B7), (D1–D7) during FF (2071–2100) for SSP245 and SSP585 respectively. [Colour figure can be viewed at wileyonlinelibrary.com]

SSP245 scenario, in the NWI region, the western part experiences lower mean relative humidity (less than 60%), a consequence of subsiding air masses and dry conditions. This drop in humidity aligns with MSLP patterns, where higher pressures in the western part result in suppressed convection and reduced moisture transport (Sobel and Maloney 2000). Conversely, the southern part of NCI enjoys comparatively high mean relative humidity (80%–85%) due to moist air advection from the Bay of Bengal. This increased humidity is consistent with lower MSLP values, supporting the convergence of moist air and subsequently enhanced precipitation (Xie et al. 2010). Whereas, within that region, mean relative humidity stands at 65%–70% in the northwestern part. This aligns with moderately higher MSLP, which favours the ascent of air masses and facilitates convection. Consequently, precipitation levels are meagre, ranging from 9 to 11 mm/day. The NEI region displays a clear gradient in mean relative humidity, closely tied to variations in MSLP, featuring high values (90%–95%) associated with lower MSLP, allowing for convergence and uplift of moist air. This leads to heavy precipitation, typically exceeding 11–13 mm/day. Conversely, the southern part (SoPI region) maintains mixed trends, limiting the ascent of air over eastern SoPI and resulting in comparatively lighter precipitation. In the WPI region, the western part exhibits mean relative humidity of 85%–90% coupled with lower MSLP, promoting convection and precipitation. Meanwhile, the eastern part maintains 80%–85% mean relative humidity, influenced by slightly higher MSLP values, resulting in reduced precipitation compared to the western part. In this context, the NWI region presents positive changes (FF-NF) of 1%–2% in mean relative humidity, concurrent with a 0.5–1 mm/day increase in precipitation, potentially related to evolving atmospheric circulation patterns. Similarly, under the SSP585 scenario, key observations include reduced humidity in the NWI region, which correlates with less precipitation and humidity variations in the other regions, impacting their precipitation regimes.

Precipitation activity over India is directly linked to the amount of moisture transport from the surrounding oceans

(Swapna and RameshKumar 2002; Levine and Turner 2012). Hence, in the NWI region, moisture transport is relatively low in the western part Figure 11a–f, aligning with the arid conditions. Conversely, the eastern part witnesses higher moisture transport values, facilitated by moisture-laden air masses originating from the Bay of Bengal. This marked difference in moisture transport is attributed to the pressure gradient and wind patterns, as higher MSLP in the west leads to divergent flow, inhibiting moisture transport; whereas lower MSLP in the east fosters convergent flow, enhancing moisture inflow and subsequently precipitation. Within the NCI region, the northwestern portion experiences elevated moisture transport, corresponding to greater precipitation levels due to ascending dry air, a consequence of the monsoon circulation, which transports moisture from the Arabian Sea. This stark contrast in moisture transport corresponds with the MSLP patterns, as lower pressures in the southeast favour the inflow of moist air and, consequently, heightened precipitation. The NEI region showcases a north-to-south gradient in moisture transport, in line with the MSLP variations. The northern part receives substantial moisture transport, driven by the convergence of air masses due to lower MSLP. This leads to heavy precipitation. Conversely, the southern part exhibits lower moisture transport values, tied to higher MSLP and subsequently lighter rainfall. Also, in the WPI region, the western part experiences notable moisture transport, consistent with lower MSLP and higher convective activity, resulting in increased precipitation. Conversely, the eastern part maintains slightly lower moisture transport, influenced by relatively higher MSLP values and, subsequently, reduced precipitation.

To elevate this study more, CAPE is computed within the altitude range of 850–700 hPa. As displayed in Figure 11g–l, the study reveals notable variations in CAPE values that have implications for convective processes and atmospheric instability. Over the NF under the SSP245, the highest CAPE values, exceeding 1800 J/kg, are prominently observed over the NEI region and the southern part of NCI. Meanwhile, CAPE values ranging from 1600 to 1800 J/kg are documented over the EPI region, the eastern sectors of WPI, the southeastern parts of NWI, and some areas of NCI. Regions with CAPE levels falling between 1400 and 1600 J/kg include SoPI, the western part of WPI, and NWI. In contrast, the western segment of NWI may experience the lowest CAPE values, dipping below 1400 J/kg. For FF, under SSP245, CAPE patterns exhibit some shifts. The NEI region still stands out with CAPE values exceeding 1800 J/kg, and parts of NCI display CAPE values between 1600 and 1800 J/kg. Additionally, the majority of the EPI region, the southwestern portions of NCI, the eastern part of NWI, and certain areas of the WPI region exhibit CAPE levels in the 1400–1600 J/kg range. Under SSP585 and in NF, the highest CAPE values, surpassing 1800 J/kg, remain consistent over the NEI and the southern part of NCI. CAPE values ranging from 1600 to 1800 J/kg are also found over the WPI region, the eastern part of NWI, the central region of EPI, and parts of the EPI region. Regions with CAPE levels in the 1400–1600 J/kg range encompass the western section of NWI, the WPI region, and the SoPI region. Examining changes in CAPE from NF to FF under SSP245 reveals that NEI, SoPI, EPI, WPI, and NWI regions exhibit changes ranging from 40 to 70 J/kg. Conversely, the NCI region experiences comparatively smaller changes,

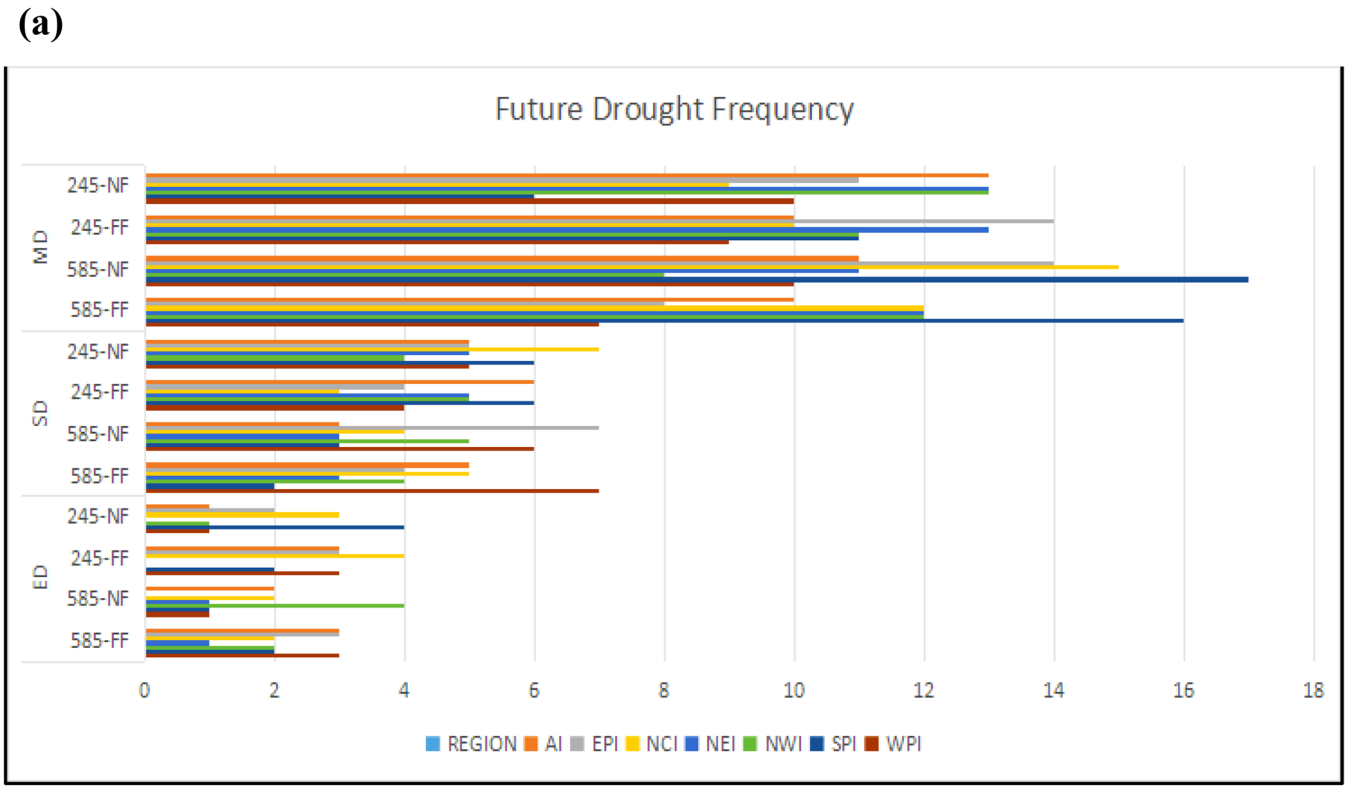

FIGURE 8 | (a) Frequency and (b) trend of drought events (Moderate, Severe, and Extreme) for NF to FF, under SSP245 and SSP585. [Colour figure can be viewed at wileyonlinelibrary.com]

(b)

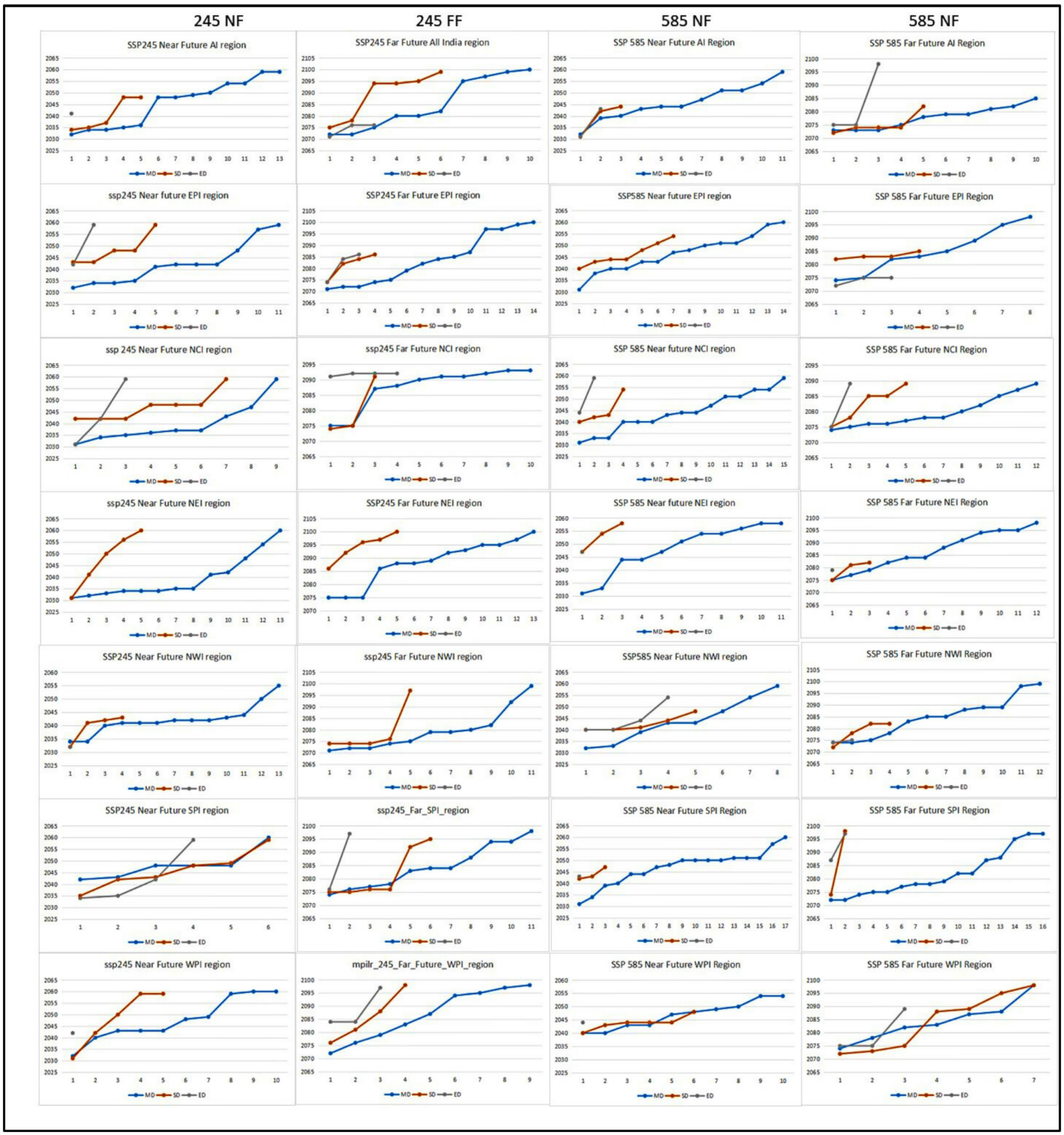

FIGURE 8 | (Continued)

with CAPE varying by less than 40 J/kg. In contrast, SSP245 shows an increase in CAPE values ranging from 130 to 160 J/kg in NEI and SoPI regions. The NWI region displays the most dramatic shifts, with CAPE changes ranging from 160 to 190 J/kg in the eastern part, 190–220 J/kg in the central region, and 220–250 J/kg in the western part. All these trends are further validated by MSE (Figure 11m–r). In NF, under SSP245, the elevated MSE values over the NCI region can be explained by the convergence of warm, moist air masses from the Bay of Bengal and the Arabian Sea (Emanuel 1994). This convergence results in an increased supply of moisture and latent heat energy, contributing to the heightened MSE and providing favourable conditions for convective processes (Trenberth and Shea 2005). The NWI region's moderate MSE values can be attributed to its proximity to the western coast and the influence of the Western Ghats, which play a role in moisture retention and advection (Seager et al. 2010). Conversely, the SoPI region exhibits lower MSE values due to its location in the rain shadow of the Western Ghats. This topographical feature inhibits the influx of moist air masses, leading to reduced MSE and, consequently,

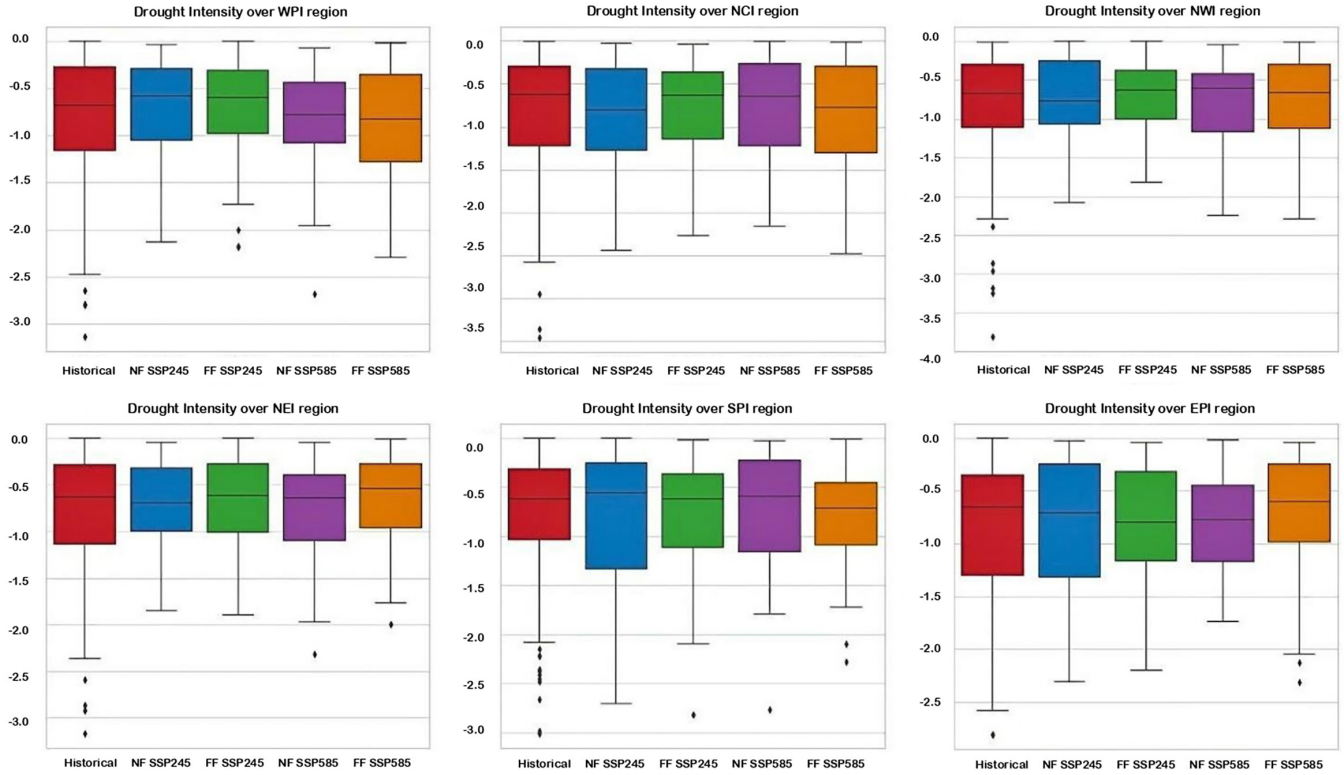

FIGURE 9 | Box plots of drought indicator of SPI across different regions of India for different time slices under two SSP scenarios. Box plot components are midline, median value; box edges, 25th percentile (lower quartile) and 75th percentile (upper quartile); upper whisker = min (max(*x*), Q3 + 1.5 9 IQR), where *x* axis is the set of data values, Q3 is the upper quartile and IQR is the interquartile range; lower whisker = max(min(*x*), Q1 + 1.5 9 IQR); and points, outliers. [Colour figure can be viewed at wileyonlinelibrary.com]

decreased potential for convective activity. These dynamics, along with the prevailing atmospheric circulation patterns, influence regional drought tendencies (Dee et al. 2011). When considering the SSP585 scenario, the intensification of MSE patterns is indicative of a warming climate, driven by increased greenhouse gas concentrations (Huffman et al. 1997). This intensification leads to amplified moisture transport as seen in Figure 11a–f and enhanced CAPE, primarily affecting the NWI region (Ramanathan and Collins 1991).

4 | Conclusions

This research focused on understanding key aspects of India's future climate by addressing essential questions about the frequency, intensity, and underlying mechanisms of droughts. To conduct this investigation, 10 GCMs from CMIP6 and their MME for the projection of historical drought events in India and its six homogeneous regions (EPI, NCI, NEI, NWI, SPI, WPI) spanning the period from 1901 to 2014 are employed. The reliability of future drought projections presented in this study is influenced by several factors. Whilst the use of multiple CMIP6 GCMs and MME enhances the robustness of findings by accounting for inter-model spread, certain limitations remain. These include structural differences amongst models, coarse spatial resolution that may overlook localised drought processes, and internal climate variability which may mask forced trends over shorter time frame. Now, addressing the first research question regarding the replication of precipitation patterns, the evaluation of CMIP6 models has yielded insightful findings. The comparison of model performance based on various parameters reveals a clear ranking in terms of predictive accuracy. MME emerges as the top-performing model, demonstrating the highest level of agreement with observed data. However, it is crucial to recognise the presence of biases within certain models. Notably, ACCESS-ESM1-5, CanESM5, and ACCESS-CM2 exhibit substantial biases, indicating areas for improvement in their simulation of precipitation patterns. Conversely, models such as MPI-ESM1-2-LR, MPI-ESM1-2-HR, NorESM2-MM, and the MME show fewer pronounced biases, underlining their reliability in capturing precipitation variability across the region. Thus, MME has been utilised to assess future drought events under the two SSPs: SSP245 and SSP585, during two distinct time frames: NF (2031–2060) and FF (2071–2100).

Getting into the second research question, our focus extended to the future trends of droughts. NWI and NCI stand out as potential hotspots for future drought events signalling critical periods of severe and extreme drought events in 2040, 2043, and 2054. Analysis revealed the following results:

1. Overall Trend: There is an upward trend in the frequency of extreme drought events across various regions of India as time progresses from NF to FF.
2. Regional Variances: In NWI and AI regions, there's a reduction in extreme drought events from NF to FF in both SSP scenarios. Whereas in SoPI, there's a decrease

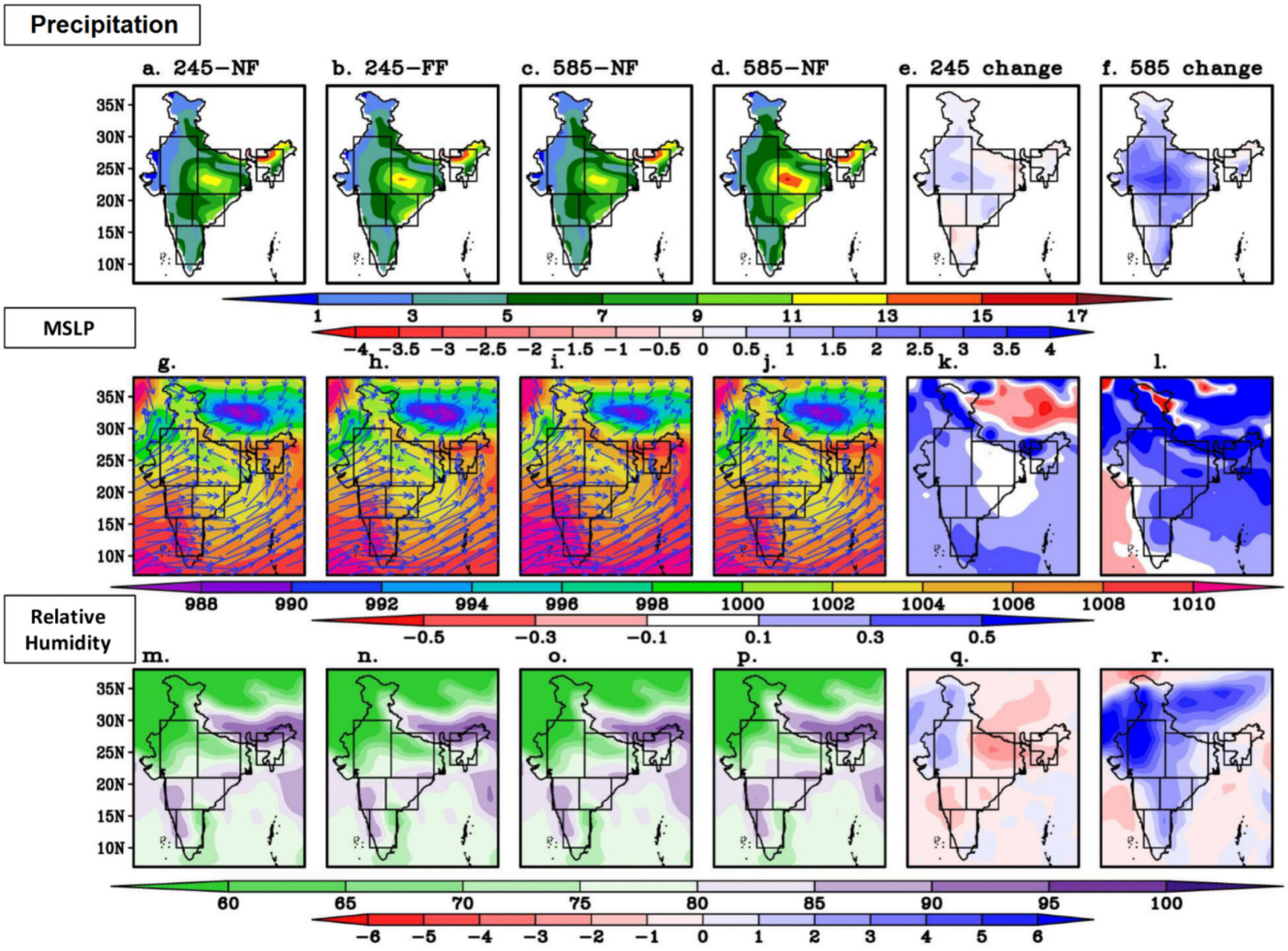

FIGURE 10 | Spatial plots of (a–f) Precipitation (*mm / day*), (g–l) Mean Sea Level Pressure (MSLP) *hPa*, (m–r) Relative Humidity during ISMR period (JJAS) under SSP245 and SSP585 for two different time slices NF and FF and their changes from NF to FF. [Colour figure can be viewed at wileyonlinelibrary.com]

in extreme drought events under SSP245 but an increase under SSP585. NEI region experiences relatively stable moderate drought events under SSP245, with a decrease anticipated under SSP585. On the other hand, there's an increase in severe drought events across India overall, but a decrease is projected in EPI region under both SSP scenarios and in NCI and WPI regions. NWI, NCI, and WPI regions may experience an increase in severe drought events under SSP585, whilst NEI region may remain relatively constant.

3. Drought Intensity and Distribution: Most severe drought conditions occur in the FF under SSP585 in WPI, NCI, and NWI regions, indicating a substantial increase in drought intensity. NEI region experiences the highest SPI values in NF under SSP585, suggesting more immediate changes in drought conditions. Similarly, SoPI and EPI regions exhibit the highest values in NF under SSP245, implying higher drought intensity and potential longer-lasting impacts.

The objective to answer the "why" behind these trends formed the core of the third research question. Parameters such as RH, moisture transport, CAPE, and MSE have been analysed to understand the core of atmospheric physics behind the future drought trends. Atmospheric instability and CAPE, particularly in the NWI region, contribute to intensified drought risks in NF and FF. Also, MSLP variations and moisture transport patterns correlate with precipitation trends, indicating the influence of regional pressure systems and moisture availability; hence, acting as the basic drought drivers. Divergent patterns across regions highlight the need for nuanced, region-specific strategies. Whilst some areas experience a reduction in extreme drought events, others face an alarming increase, underscoring the necessity for adaptive policies to address evolving drought dynamics. In terms of impacts, the projected increase in drought frequency and severity poses serious risks for India's water resources, agriculture, and energy sectors. Regions such as NWI and NCI, which are already vulnerable due to groundwater depletion and high dependency on rainfed crops, may experience heightened food insecurity, water stress, and economic losses (Mall et al. 2006; Rodell et al. 2009; Mishra and Singh 2010). In NEI and WPI, ecological degradation, forest stress, and biodiversity loss are potential concerns, especially under the more intense scenarios (Kumar and Gautam 2014). These findings underscore the urgent need for integrated water resource

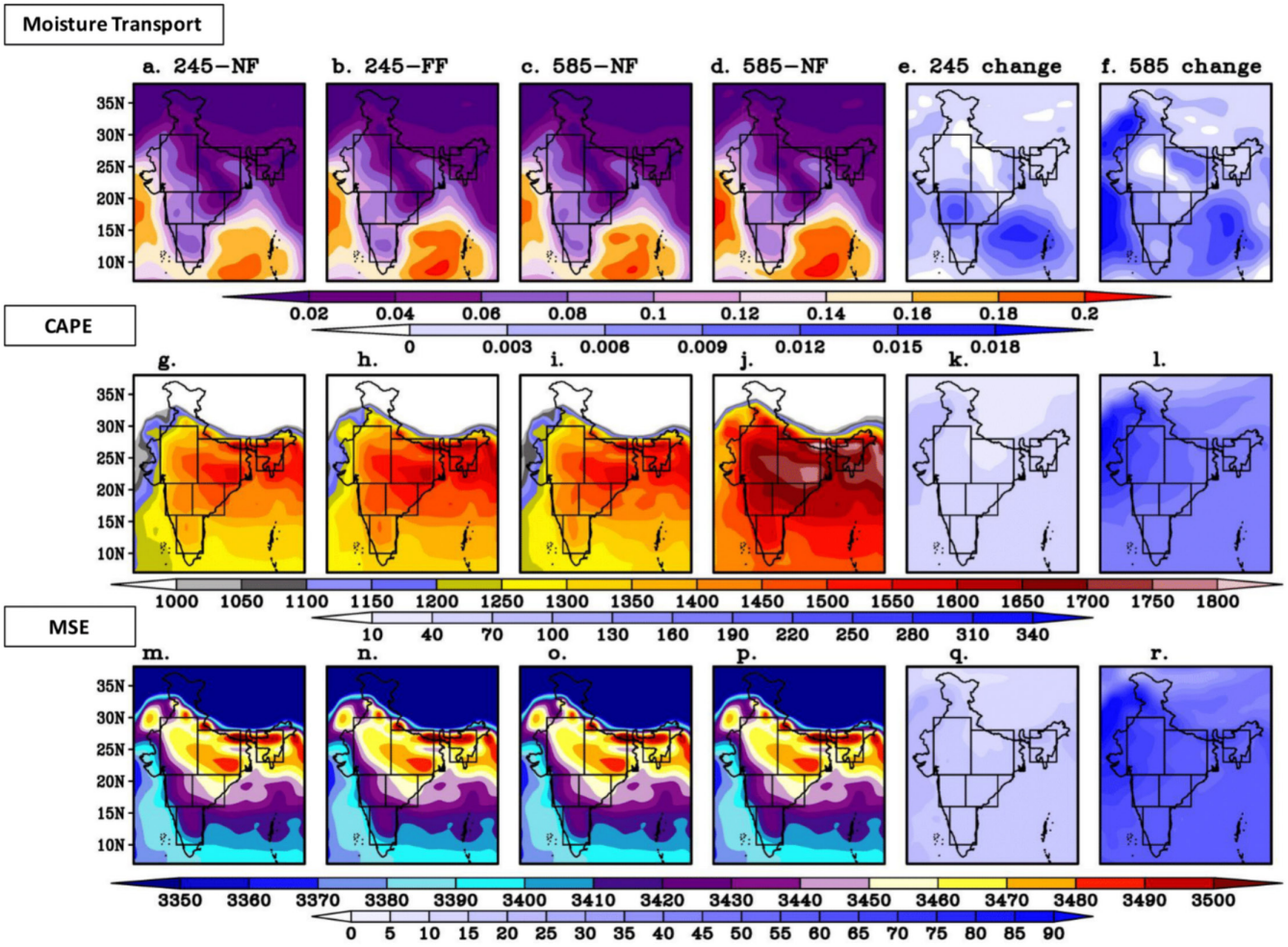

FIGURE 11 | Spatial plots of Moisture Transport ($kgm^{-1}s^{-1}$), Convective Available Potential Energy (CAPE) (J/kg), Moist Static Energy (MSE) during JJA under SSP245 and SSP585 for two different time slices NF and FF and their changes from NF to FF. [Colour figure can be viewed at wileyonlinelibrary.com]

management, drought-resilient agriculture, and early warning systems to build regional resilience.

Author Contributions

Rajeev Bhatla: conceptualization, methodology, supervision, project administration, resources, writing – review and editing. **Aashna Verma:** data curation, investigation, formal analysis, conceptualization, writing – original draft, methodology, validation. **Akash Vishwakarma:** data curation, formal analysis, investigation, methodology. **R. K. Mall:** writing – review and editing, supervision, investigation.

Acknowledgments

This research project is an integral component of an R&D initiative generously backed by the Science and Engineering Research Board (DST-SERB), Government of India. We wish to convey our sincere appreciation to the India Meteorology Department (IMD) for their invaluable support in supplying high-resolution gridded datasets. Furthermore, our gratitude extends to the World Climate Research Programme (WCRP) for their pivotal role in providing access to CMIP6 datasets.

Conflicts of Interest

The authors declare no conflicts of interest.

Data Availability Statement

Data relevant to this research can be openly downloaded from the websites listed below:

IMD Precipitation: https://www.imdpune.gov.in/cmpg/Griddata/Rainfall_25_NetCDF.html.

CMIP6 datasets: The open-source link for accessing CMIP6 simulations through ESGF is https://esgf-node.llnl.gov/search/cmip6/. There are different models to choose from 'Source I' filter panel. To locate precipitation data, users are advised to choose the variable "pr" (indicating precipitation) and set the frequency to daily. Additionally, users should select the Experiment ID as historical or for different SSP scenarios (SSP245 & SSP585 for this study) and refer to Table 2 in the paper for a concise description of the CMIP6 models utilised in this study. Finally, download the netCDF (.nc) files that appear as search outputs.

References

AghaKouchak, A., A. Farahmand, F. S. Melton, et al. 2015. "Remote Sensing of Drought: Progress, Challenges and Opportunities." *Reviews of Geophysics* 53, no. 2: 452–480.

Ayugi, B., Z. W. Shilenje, H. Babaousmail, et al. 2022. "Projected Changes in Meteorological Drought Over East Africa Inferred From Bias-Adjusted CMIP6 Models." *Natural Hazards* 113, no. 2: 1151–1176.

Bhatla, R., S. Ghosh, S. Verma, R. K. Mall, and G. R. Gharde. 2019. "Variability of Monsoon Over Homogeneous Regions of India Using Regional Climate Model and Impact on Crop Production." *Agricultural Research* 8: 331–346.

Bhatla, R., S. Verma, S. Ghosh, and R. K. Mall. 2020. "Performance of Regional Climate Model in Simulating Indian Summer Monsoon Over Indian Homogeneous Region." *Theoretical and Applied Climatology* 139: 1121–1135.

Bi, D., M. Dix, S. Marsland, et al. 2020. "Configuration and Spin-Up of ACCESS-CM2, the New Generation Australian Community Climate and Earth System Simulator Coupled Model." *Journal of Southern Hemisphere Earth Systems Science* 70, no. 1: 225–251.

Bisht, D. S., V. Sridhar, A. Mishra, C. Chatterjee, and N. S. Raghuwanshi. 2019. "Drought Characterization Over India Under Projected Climate Scenario." *International Journal of Climatology* 39, no. 4: 1889–1911.

Cook, B. I., J. S. Mankin, K. Marvel, A. P. Williams, J. E. Smerdon, and K. J. Anchukaitis. 2020. "Twenty-First Century Drought Projections in the CMIP6 Forcing Scenarios." *Earth's Future* 8, no. 6: e2019EF001461.

Dee, D. P., S. M. Uppala, A. J. Simmons, et al. 2011. "The ERA-Interim Reanalysis: Configuration and Performance of the Data Assimilation System." *Quarterly Journal of the Royal Meteorological Society* 137, no. 656: 553–597.

Dixit, S., and K. V. Jayakumar. 2022. "Spatio-Temporal Analysis of Copula-Based Probabilistic Multivariate Drought Index Using CMIP6 Model." *International Journal of Climatology* 42, no. 8: 4333–4350.

Edwards, D. C., and T. B. McKee. 1997. *Characteristics of 20th Century Drought in the United States at Multiple Time Scales*. Vol. 97, 155. Colorado State University.

Emanuel, K. A. 1994. *Atmospheric Convection*. Oxford University Press.

Eyring, V., S. Bony, G. A. Meehl, et al. 2016. "Overview of the Coupled Model Intercomparison Project Phase 6 (CMIP6) Experimental Design and Organization." *Geoscientific Model Development* 9, no. 5: 1937–1958.

Farahmand, A., and A. AghaKouchak. 2015. "A Generalized Framework for Deriving Nonparametric Standardized Drought Indicators." *Advances in Water Resources* 76: 140–145.

Gocic, M., and S. Trajkovic. 2013. "Analysis of Precipitation and Drought Data in Serbia Over the Period 1980–2010." *Journal of Hydrology* 494: 32–42.

Hao, Z., and A. AghaKouchak. 2013. "Multivariate Standardized Drought Index: A Parametric Multi-Index Model." *Advances in Water Resources* 57: 12–18.

He, B., A. Lü, J. Wu, L. Zhao, and M. Liu. 2011. "Drought Hazard Assessment and Spatial Characteristics Analysis in China." *Journal of Geographical Sciences* 21: 235–249.

Held, I. M., and B. J. Soden. 2006. "Robust Responses of the Hydrological Cycle to Global Warming." *Journal of Climate* 19, no. 21: 5686–5699.

Huffman, G. J., R. F. Adler, P. Arkin, et al. 1997. "The Global Precipitation Climatology Project (GPCP) Combined Precipitation Dataset." *Bulletin of the American Meteorological Society* 78, no. 1: 5–20.

Konda, G., and N. K. Vissa. 2023. "Evaluation of CMIP6 Models for Simulations of Surplus/Deficit Summer Monsoon Conditions Over India." *Climate Dynamics* 60, no. 3–4: 1023–1042.

Krishnamurti, T. N., and H. N. Bhalme. 1976. "Oscillations of a Monsoon System. Part I. Observational Aspects." *Journal of Atmospheric Sciences* 33, no. 10: 1937–1954.

Krishnan, R., C. Gnanaseelan, J. Sanjay, et al. 2020. "Introduction to Climate Change Over the Indian Region." In *Assessment of Climate Change Over the Indian Region: A Report of the Ministry of Earth Sciences (MoES), Government of India*, 1–20. Springer Singapore.

Krishnan, R., P. Swapna, R. Vellore, et al. 2019. "The IITM Earth System Model (ESM): Development and Future Roadmap." In *Current Trends in the Representation of Physical Processes in Weather and Climate Models*, 183–195. Springer Singapore.

Kumar, P., and P. P. Sarthi. 2021. "Intraseasonal Variability of Indian Summer Monsoon Rainfall in CMIP6 Models Simulation." *Theoretical and Applied Climatology* 145, no. 1–2: 687–702.

Kumar, R., and H. R. Gautam. 2014. "Climate Change and Its Impact on Agricultural Productivity in India." *Journal of Climatology & Weather Forecasting* 2, no. 1: 1–3.

Levine, R. C., and A. G. Turner. 2012. "Dependence of Indian Monsoon Rainfall on Moisture Fluxes Across the Arabian Sea and the Impact of Coupled Model Sea Surface Temperature Biases." *Climate Dynamics* 38: 2167–2190.

Lin, M., and P. Huybers. 2019. "If Rain Falls in India and No One Reports it, Are Historical Trends in Monsoon Extremes Biased?" *Geophysical Research Letters* 46, no. 3: 1681–1689.

Lloyd-Hughes, B. 2014. "The Impracticality of a Universal Drought Definition." *Theoretical and Applied Climatology* 117: 607–611.

Mall, R. K., A. Gupta, R. Singh, R. S. Singh, and L. S. Rathore. 2006. "Water Resources and Climate Change: An Indian Perspective." *Current Science* 90, no. 12: 1610–1626.

Mallya, G., V. Mishra, D. Niyogi, S. Tripathi, and R. S. Govindaraju. 2016. "Trends and Variability of Droughts Over the Indian Monsoon Region." *Weather and Climate Extremes* 12: 43–68.

Mauritsen, T., J. Bader, T. Becker, et al. 2019. "Developments in the MPI-M Earth System Model Version 1.2 (MPI-ESM1. 2) and Its Response to Increasing CO2." *Journal of Advances in Modeling Earth Systems* 11, no. 4: 998–1038.

McKee, T. B., N. J. Doesken, and J. Kleist. 1993. "The Relationship of Drought Frequency and Duration to Time Scales." In *Proceedings of the 8th Conference on Applied Climatology*, 179–183. American Meteorological Society.

Meehl, G. A., G. J. Boer, C. Covey, M. Latif, and R. J. Stouffer. 1997. "Intercomparison Makes for a Better Climate Model." *Eos, Transactions American Geophysical Union* 78, no. 41: 445–451.

Meehl, G. A., G. J. Boer, C. Covey, M. Latif, and R. J. Stouffer. 2000. "The Coupled Model Intercomparison Project (CMIP)." *Bulletin of the American Meteorological Society* 81, no. 2: 313–318.

Mishra, A., and S. C. Liu. 2014. "Changes in Precipitation Pattern and Risk of Drought Over India in the Context of Global Warming." *Journal of Geophysical Research: Atmospheres* 119, no. 13: 7833–7841.

Mishra, A. K., and V. P. Singh. 2010. "A Review of Drought Concepts." *Journal of Hydrology* 391, no. 1–2: 202–216.

Müller, W. A., J. H. Jungclaus, T. Mauritsen, et al. 2018. "A Higher-Resolution Version of the Max Planck Institute Earth System Model (MPI-ESM1. 2-HR)." *Journal of Advances in Modeling Earth Systems* 10, no. 7: 1383–1413.

Nagarajan, R. 2003. *Drought: Assessment, Monitoring, Management and Resources Conservation*. Capital Publishing Company.

O'Neill, B. C., C. Tebaldi, D. P. Van Vuuren, et al. 2016. "The Scenario Model Intercomparison Project (ScenarioMIP) for CMIP6." *Geoscientific Model Development* 9, no. 9: 3461–3482.

Pai, D. S., M. Rajeevan, O. P. Sreejith, B. Mukhopadhyay, and N. S. Satbha. 2014. "Development of a New High Spatial Resolution (0.25×0.25) Long Period (1901-2010) Daily Gridded Rainfall Data Set Over India and Its Comparison With Existing Data Sets Over the Region." *Mausam* 65, no. 1: 1–18.

Papalexiou, S. M., C. R. Rajulapati, K. M. Andreadis, E. Foufoula-Georgiou, M. P. Clark, and K. E. Trenberth. 2021. "Probabilistic

Evaluation of Drought in CMIP6 Simulations." *Earth's Future* 9, no. 10: e2021EF002150.

Parthasarathy, B., A. A. Munot, and D. R. Kothawale. 1994. "All-India Monthly and Seasonal Rainfall Series: 1871–1993." *Theoretical and Applied Climatology* 49: 217–224.

Preethi, B., R. Ramya, S. K. Patwardhan, M. Mujumdar, and R. H. Kripalani. 2019. "Variability of Indian Summer Monsoon Droughts in CMIP5 Climate Models." *Climate Dynamics* 53: 1937–1962.

Rajeevan, M., J. Bhate, and A. K. Jaswal. 2008. "Analysis of Variability and Trends of Extreme Rainfall Events Over India Using 104 Years of Gridded Daily Rainfall Data." *Geophysical Research Letters* 35, no. 18: 2008GL035143.

Ramanathan, V., and W. Collins. 1991. "Thermodynamic Regulation of Ocean Warming by Cirrus Clouds Deduced From Observations of the 1987 El Niño." *Nature* 351, no. 6321: 27–32.

Reddy, N. M., and S. Saravanan. 2023. "Extreme Precipitation Indices Over India Using CMIP6: A Special Emphasis on the SSP585 Scenario." *Environmental Science and Pollution Research* 30, no. 16: 47119–47143.

Rodell, M., I. Velicogna, and J. S. Famiglietti. 2009. "Satellite-Based Estimates of Groundwater Depletion in India." *Nature* 460, no. 7258: 999–1002.

Roxy, M. K., S. Ghosh, A. Pathak, et al. 2017. "A Threefold Rise in Widespread Extreme Rain Events Over Central India." *Nature Communications* 8, no. 1: 1–11.

Seager, R., N. Naik, and G. A. Vecchi. 2010. "Thermodynamic and Dynamic Mechanisms for Large-Scale Changes in the Hydrological Cycle in Response to Global Warming." *Journal of Climate* 23, no. 17: 4651–4668.

Seland, Ø., M. Bentsen, D. Olivié, et al. 2020. "Overview of the Norwegian Earth System Model (NorESM2) and Key Climate Response of CMIP6 DECK, Historical, and Scenario Simulations." *Geoscientific Model Development* 13, no. 12: 6165–6200.

Sharma, A., and M. K. Goyal. 2020. "Assessment of Drought Trend and Variability in India Using Wavelet Transform." *Hydrological Sciences Journal* 65, no. 9: 1539–1554.

Singh, A. K., J. N. Tripathi, K. K. Singh, V. Singh, and M. Sateesh. 2019. "Comparison of Different Satellite-Derived Rainfall Products With IMD Gridded Data Over Indian Meteorological Subdivisions During Indian Summer Monsoon (ISM) 2016 at Weekly Temporal Resolution." *Journal of Hydrology* 575: 1371–1379.

Singh, N., and N. A. Sontakke. 1999. "On the Variability and Prediction of Rainfall in the Post-Monsoon Season Over India." *International Journal of Climatology: A Journal of the Royal Meteorological Society* 19, no. 3: 309–339.

Sobel, A. H., and E. D. Maloney. 2000. "Effect of ENSO and the MJO on Western North Pacific Tropical Cyclones." *Geophysical Research Letters* 27, no. 12: 1739–1742.

Soni, A. K., J. N. Tripathi, M. Tewari, M. Sateesh, and T. Singh. 2023. "Future Projection of Drought Risk Over Indian Meteorological Subdivisions Using Bias-Corrected CMIP6 Scenarios." *Atmosphere* 14, no. 4: 725.

Sontakke, N. A., and N. Singh. 1996. "Longest Instrumental Regional and All-India Summer Monsoon Rainfall Series Using Optimum Observations: Reconstruction and Update." *Holocene* 6, no. 3: 315–331.

Swapna, P., and M. R. RameshKumar. 2002. Role of Low Level Flow on the Summer Monsoon Rainfall Over the Indian Subcontinent During Two Contrasting Monsoon Years.

Swart, N. C., J. N. Cole, V. V. Kharin, et al. 2019. "The Canadian Earth System Model Version 5 (CanESM5. 0.3)." *Geoscientific Model Development* 12, no. 11: 4823–4873.

Tatebe, H., T. Ogura, T. Nitta, et al. 2019. "Description and Basic Evaluation of Simulated Mean State, Internal Variability, and Climate Sensitivity in MIROC6." *Geoscientific Model Development* 12, no. 7: 2727–2765.

Taylor, K. E. 2001. "Summarizing Multiple Aspects of Model Performance in a Single Diagram." *Journal of Geophysical Research: Atmospheres* 106, no. D7: 7183–7192.

Touma, D., M. Ashfaq, M. A. Nayak, S. C. Kao, and N. S. Diffenbaugh. 2015. "A Multi-Model and Multi-Index Evaluation of Drought Characteristics in the 21st Century." *Journal of Hydrology* 526: 196–207.

Trenberth, K. E. 1999. "Conceptual Framework for Changes of Extremes of the Hydrological Cycle With Climate Change." *Climatic Change* 42, no. 1: 327–339.

Trenberth, K. E., and D. J. Shea. 2005. "Relationships Between Precipitation and Surface Temperature." *Geophysical Research Letters* 32, no. 14: L14703.

Van Loon, A. F. 2015. "Hydrological Drought Explained." *Wiley Interdisciplinary Reviews: Water* 2, no. 4: 359–392.

Verma, A., A. Vishwakarma, S. Bist, S. Kumar, and R. Bhatla. 2023. "A Long-Term Drought Assessment Over India Using CMIP6 Framework: Present and Future Perspectives: Drought Assessment Over India Using CMIP6." *Mausam* 74, no. 4: 963–972.

Verma, S., R. Bhatla, N. K. Shahi, and R. K. Mall. 2022. "Regional Modulating Behavior of Indian Summer Monsoon Rainfall in Context of Spatio-Temporal Variation of Drought and Flood Events." *Atmospheric Research* 274: 106201.

Wang, B., R. Wu, and K. M. Lau. 2001. "Interannual Variability of the Asian Summer Monsoon: Contrasts Between the Indian and the Western North Pacific–East Asian Monsoons." *Journal of Climate* 14, no. 20: 4073–4090.

Wang, T., X. Tu, V. P. Singh, X. Chen, and K. Lin. 2021. "Global Data Assessment and Analysis of Drought Characteristics Based on CMIP6." *Journal of Hydrology* 596: 126091.

Wilhite, D. A., and M. H. Glantz. 1985. "Understanding: The Drought Phenomenon: The Role of Definitions." *Water International* 10, no. 3: 111–120.

Xie, S. P., C. Deser, G. A. Vecchi, J. Ma, H. Teng, and A. T. Wittenberg. 2010. "Global Warming Pattern Formation: Sea Surface Temperature and Rainfall." *Journal of Climate* 23, no. 4: 966–986.

Xu, K., D. Yang, H. Yang, Z. Li, Y. Qin, and Y. Shen. 2015. "Spatio-Temporal Variation of Drought in China During 1961–2012: A Climatic Perspective." *Journal of Hydrology* 526: 253–264.

Yukimoto, S., H. Kawai, T. Koshiro, et al. 2019. "The Meteorological Research Institute Earth System Model Version 2.0, MRI-ESM2. 0: Description and Basic Evaluation of the Physical Component." *Journal of the Meteorological Society of Japan. Ser. II* 97, no. 5: 931–965.

Zargar, A., R. Sadiq, B. Naser, and F. I. Khan. 2011. "A Review of Drought Indices." *Environmental Reviews* 19: 333–349.

Ziehn, T., M. A. Chamberlain, R. M. Law, et al. 2020. "The Australian Earth System Model: ACCESS-ESM1.5." *Journal of Southern Hemisphere Earth Systems Science* 70, no. 1: 193–214.